



New Particle Formation in the Tropical Free Troposphere during CAMP²Ex: Statistics and Impact of Emission Sources, Convective activity, and Synoptic Condition

5 Qian Xiao¹, Jiaoshi Zhang¹, Yang Wang², Luke D. Ziemba³, Ewan Crosbie^{3,4}, Edward L. Winstead³, Claire E. Robinson³, Joshua P. DiGangi³, Glenn S. Diskin³, Jeffrey S. Reid⁵, K. Sebastian Schmidt⁶, Armin Sorooshian^{7,8}, Miguel Ricardo A. Hilario⁸, Sarah Woods⁹, Paul Lawson⁹, Snorre A. Starnes³, Jian Wang¹

¹Department of Energy, Environmental and Chemical Engineering, Washington University in St. Louis, St. Louis, MO 63130, USA

10 ²Department of Chemical, Environmental and Materials Engineering, University of Miami, Coral Gables, FL 33124, USA

³NASA Langley Research Center, Hampton, VA 23666, USA

⁴Science Systems and Applications, Inc., Hampton, VA 23666, USA

⁵Marine Meteorology Division, Naval Research Laboratory, Monterey, CA, USA

15 ⁶Laboratory for Atmospheric and Space Physics, University of Colorado, Boulder, CO 80309, USA

⁷Department of Chemical and Environmental Engineering, University of Arizona, Tucson, AZ, 85721, USA

⁸Department of Hydrology and Atmospheric Sciences, University of Arizona, Tucson, AZ 85721, USA

⁹Stratton Park Engineering Company (SPEC), Boulder, CO 80301, USA

Correspondence to: Jian Wang (jian@wustl.edu)

20

Abstract. Nucleation in the free troposphere (FT) and subsequent growth of new particles represents a globally important source of cloud condensation nuclei (CCN). Whereas new particle formation (NPF) has been shown to occur frequently in the upper troposphere over tropical oceans, there have been few studies of NPF at lower altitudes over the tropical marine environment. In addition, the impact of anthropogenic emissions and biomass burning on NPF over the tropics remains poorly understood. In this study, we examine NPF in the lower and mid troposphere (3-8.5 km) over ocean and coastal regions of the Sulu Sea and Northern Subtropical Pacific Ocean in Southeast Asia using airborne measurements during the recent Cloud, Aerosol and Monsoon Processes Philippines Experiment (CAMP²Ex). CAMP²Ex took place from 25 August through 5 October 2019, including both late southwest monsoon and monsoon transition. Recent NPF events, as evidenced by elevated concentrations of newly formed particles (i.e., particles of diameters between 3 and 10 nm), were observed during 4% of the total flight time (5 out of 128 hours). The frequency of NPF increases with altitude, reaching 49% above an altitude of 8 km. NPF was mostly observed at altitudes above 3 km and coincided with elevated relative humidity (RH), suggesting that NPF is closely associated with convective cloud outflow in conditions of low temperature and reduced pre-existing particle concentrations. Air masses are categorized into background, biomass burning-influenced, and urban-influenced air based on in-situ CO, CH₄ and O₃ measurements. NPF in background air was mostly observed above 6 km, typically accompanied by the lowest surface area among all air mass types. NPF occurred above the 0 °C level at 5.5-7 km in air masses influenced by convectively detrained biomass burning and/or urban emissions and was enhanced by 1) scavenged primary particles; 2) elevated precursor concentrations and 3) enhanced irradiance due to cloud

25
30
35



reflections. However, NPF was suppressed in aged urban influenced air masses where the reactive precursors were
40 mostly consumed while existing particle surface area remained relatively high due to longer aerosol lifetimes in the
free troposphere. The results highlight the role of convective clouds that efficiently scavenge existing aerosol
particles, inject reactive precursors into free troposphere, and enhance UV irradiance, all of which facilitate NPF.
This study also illustrates the competing influences of different variables and complex interactions between
anthropogenic emissions, transport, convective clouds, and meteorology, which lead to NPF under a variety of
45 conditions and at different altitudes in tropical marine environment.

1 Introduction

New particle formation (NPF), the process of gas to particle nucleation and early growth to 2-3 nm, has been
observed in many regions and over a wide range of altitudes, i.e., from the pristine to heavily polluted environment,
from the tropics to the Arctic, and from boundary layer (BL) to tropopause layer (TL) (Chae et al., 2011; Twohy et
50 al., 2002; Dada et al., 2017; Andreae et al., 2018; Kerminen et al., 2018; Zheng et al., 2021; Reid et al., 2016).
Modelling studies suggest that on a global average NPF contributes up to approximately half of the cloud
condensation nuclei (CCN) in the troposphere (Gordon et al., 2017), and strongly influences cloud formation and
climate (Kulmala et al., 2014). The rate of NPF depends on the concentrations of low volatility vapors (e.g., H₂SO₄
and highly oxygenated organics) that participate in the NPF, and the rate is also a function of temperature. As these
55 low volatility vapors are mostly formed by photochemistry, their concentrations depend on the intensity of solar
radiation as well as the concentration of precursors. Essentially all long-term surface measurements show that the
average solar radiation intensity is stronger during NPF event days compared with non-event days. Pre-existing
aerosol particles serve as both a condensational sink for the low volatility vapors and a coagulation sink for newly
formed particles, therefore they are expected to inhibit NPF. Indeed, observations at many locations have shown that
60 new particle events in the troposphere typically occur under clean conditions (Kerminen et al., 2018; Kuang et al.,
2009).

Over the oceans, NPF is typically observed in the free troposphere (FT). It had been long thought that NPF rarely
occurs within the remote marine boundary layer, because primary sea spray aerosols (SSA) present large
condensation and coagulation sinks (Pirjola et al., 2000). A recent study shows that NPF takes place regularly in the
65 upper part of the decoupled marine boundary layer following the passage of cold fronts over mid-latitude ocean, due
to the combination of low existing aerosol loading, cold temperature, availability of reactive gases, and high actinic
fluxes in the clear regions between scattered cumulus clouds (Zheng et al., 2021). In boundary layer over coastal
regions, NPF can occur in continental outflow such as transported urban plumes (Reid et al., 2016). In the FT over
tropical and mid-latitude oceans, NPF was mostly observed in the air mass processed by convective clouds (Clarke
70 et al., 1998; Clarke et al., 1999; Perry and Hobbs, 1994; Williamson et al., 2019). Intense NPF in convective outflow
regions was observed in the tropical upper troposphere over both Pacific and Atlantic oceans (Williamson et al.,
2019). Chemical-transport model simulations indicate this NPF in the tropical upper troposphere is a globally
important source of CCN in the lower troposphere. In the outflow of convective clouds, existing particles are



75 depleted due to wet scavenging, leading to low condensation and coagulation sinks that promote NPF. At the same
time, reactive gases such as dimethyl sulfide (DMS) are transported from marine boundary layer to the outflow
region, where the actinic flux is high and the reactive gases react to form low volatility species that participate in
NPF (Williamson et al., 2019). Concurrent observations of elevated H₂SO₄ vapor concentration with the newly
formed particles over the open ocean suggest that H₂SO₄ formed from oxidation of DMS likely plays an important
role in NPF. While NH₃ and highly oxygenated compounds (HOM) can participate in NPF, modeling studies have
80 shown that between 5.8 km altitude and the top of the troposphere, on average globally, about 80% of NPF at these
altitudes involves only sulfuric acid and water (binary nucleation; Gordon et al., 2017), and a large fraction of the
NPF is ion-induced, especially over oceans where the overall NPF rate is relatively low (Dunne et al., 2016; Gordon
et al., 2017). In addition to cloud outflow regions, newly formed particles were also observed in the FT near the
edge of cumulus clouds with enhanced actinic flux (Wehner et al., 2015), and in continental outflow just above the
85 boundary layer cloud top (i.e., lower FT) over the northwestern Atlantic (Corral et al., 2022) and northeastern
Pacific (Dadashazar et al., 2018).

Previous studies have greatly advanced our understanding of NPF in the marine environment. Over tropical oceans,
most studies focused on the NPF in the upper troposphere (UT), whereas the observations of NPF in the outflow of
convective clouds in the middle FT (i.e., 4–8 km) remain scarce (Clarke et al., 1998; Williamson et al., 2019). Model
90 simulation from the perspective of galactic cosmic rays suggests that aerosol formation in the lower and middle
troposphere is weak, while the strongest aerosol formation takes place in upper troposphere over tropic ocean (Kazil
et al., 2006). In addition, previous measurements were mostly carried out in pristine environments. As a result, the
impact of anthropogenic emissions on NPF over tropical oceans is still poorly understood. In this study, we take
advantage of comprehensive airborne measurements during the Cloud, Aerosol and Monsoon Processes Philippines
95 Experiment (CAMP²Ex) to investigate NPF from the lower (~3 km) to upper FT (~8.5 km) in both background air
masses and those impacted by urban emissions and biomass burning. The monsoon transition was captured during
CAMP²Ex, allowing us to examine the impact of both changing air mass origins and convective activity on NPF.
Through both statistical analysis and case studies, we quantify the frequency of NPF and the conditions under which
NPF occurs in different air masses and their dependence on altitude. These results help improve the understanding
100 of NPF in tropical marine environments, both in background conditions and under the influence from anthropogenic
emissions.

2 Methodology

2.1 Measurements Onboard the Aircraft

The Cloud, Aerosol and Monsoon Processes Philippines Experiment (CAMP²Ex), with the objective of
105 characterizing the role of anthropogenic and natural aerosols in aerosol-cloud interaction in the vicinity of
Philippines, included deployments onboard both the NASA P-3B aircraft and SPEC Learjet 35A (Reid et al.,
submitted). The data analyzed in this study are all from the NASA P-3B aircraft, which flew 19 research flights



(flight tracks were superimposed on map as shown in Fig. S1) from 24 August to 5 October 2019, covering South China Sea (SCS), Sulu Sea, West Pacific, and the continental FT. The CAMP²Ex campaign provided an excellent
110 dataset to investigate NPF from the lower to upper troposphere (3–8.5 km) in a range of air masses, including background air and those influenced by Borneo biomass burning smoke, Asian pollution, and local emissions from Philippines (Hilario et al., 2021).

The measurements examined in this study include aerosol properties, carbon monoxide (CO), methane (CH₄) and ozone (O₃) mixing ratios, meteorological parameters, and radiation (see Table 1 for details). Two condensation
115 particle counters (CPCs, Model 3756 and 3772, TSI Inc.; Hermann et al., 2007) measured the total number concentrations of particles nominally larger than ~3 and ~10 nm ($N_{>3\text{ nm}}$ and $N_{>10\text{ nm}}$), respectively. Aerosol size distributions were characterized by a fast integrated mobility spectrometer (FIMS, 10–600 nm; Wang et al., 2017a; Wang et al., 2017b; Wang et al., 2018) and a laser aerosol spectrometer (LAS, Model 3340, TSI Inc., 100–3000 nm). The cloud droplet spectra were measured by a fast cloud droplet probe (FCDP, SPEC Inc.; Lawson et al., 2017).
120 Several trace gases measured in-situ onboard the P-3B are used to identify different air mass origins. CO and CH₄ mixing ratios were characterized by a dried-airstream near-infrared cavity ring-down absorption spectrometer (Model G2401-m, PICARRO Inc.; Digangi et al., 2021; Baier et al., 2020). O₃ was measured by a dual-beam UV adsorption sensor (Model 205; 2B Technologies; Digangi et al., 2021). Water vapor mixing ratio and relative humidity (RH) were given by a diode laser hygrometer at 1 Hz (DLH; Diskin et al., 2002; Podolske et al., 2003).
125 Upwelling and downwelling shortwave irradiance from 350–2150 nm were measured by the solar spectral flux radiometer (SSFR; Norgren et al., 2022; Schmidt et al., 2021; Chen et al., 2021).

Table 1. Information on instruments involved in NPF analysis.

Parameter/Variable	Instruments/Methods	Sampling frequency
Aerosol number concentration (> 3 nm)	Condensation particle counter (CPC, TSI-3756)	1 Hz
Number concentration of non-volatile particles (> 10 nm)	Condensation particle counter (CPC, TSI-3772) downstream of a thermodenuder	1 Hz
Aerosol size distribution (10–600 nm)	Fast integrated mobility spectrometer (FIMS)	1 Hz
Aerosol size distribution (100–3000 nm)	Laser aerosol spectrometer (LAS, TSI-3340)	1 Hz
Cloud droplet size distribution (2–50 μm)	Fast cloud droplet probe (FCDP, SPEC Inc.)	1 Hz
Ozone mixing ratio	Dual cell broadband UV absorption spectrometry (2B Technologies, Model 205)	0.4 Hz
CO and methane mixing ratio (dry mass fraction)	Near-IR cavity ringdown absorption spectroscopy (PICARRO Inc., G2401-M)	0.4 Hz



Relative humidity with respect to water (RH)	Diode laser hygrometer (DLH, NASA Langley Research Center)	1 Hz
Upwelling and downwelling shortwave irradiance	Solar spectral flux spectrometer (SSFR)	1 Hz
Latitude/longitude/GPS altitude	Litton 251	1 Hz
Air temperature	Rosemont 102 Fast	1 Hz

When P-3B was inside clouds, aerosol measurements were impacted by shattering of cloud droplets and/or ice particles on the iso-kinetic aerosol sampling inlet. The in-cloud periods and additional 3-second buffer time immediately before and after in-cloud periods were identified based on hydrometeor measurements (i.e., cloud flag, available in CAMP²Ex data archive <https://asdc.larc.nasa.gov/project/CAMP2Ex>). Aerosol measurements during the flagged periods were excluded from the analysis to minimize the influence of the measurement artifacts. Total aerosol surface area concentration was derived from the combined size distribution from multiple instruments, including FIMS and LAS, which collectively cover the size range of 10-3000 nm. All aerosol (number and surface area) concentrations and size distributions are reported at standard temperature and pressure (STP). As there was no direct measurement of actinic flux, which reflects the intensity of photo-oxidations, we calculated the ultraviolet (UV) irradiance by integrating the measured irradiance over the wavelength range of 350-400 nm from the SSFR and used it as a proxy. The total UV irradiances were derived as the sum of both upwelling and downwelling components. Examining both upwelling and downwelling components also provides insights into the factors that influence the total UV irradiance and thus photochemistry during the NPF periods.

2.2 Identification of NPF Events

In this study, we used the concentration ratio of the particles with diameter above 3 nm ($N_{>3 \text{ nm}}$) to that above 10 nm ($N_{>10 \text{ nm}}$) to identify NPF events, following a similar approach described by Zheng et al (2021). A ratio ($N_{>3 \text{ nm}}/N_{>10 \text{ nm}}$) substantially above 1 indicates the presence of newly formed particles between 3 and 10 nm, and thus a recent NPF event. Considering the response times of the CPCs to step changes in particle concentration (i.e., about 2 seconds to reach 90% of concentration step change), we first averaged the 1-second measurements of particle number concentrations (i.e., $N_{>3 \text{ nm}}$ and $N_{>10 \text{ nm}}$) into 10-s intervals. For each of the 10-s intervals, the ratio of average $N_{>3 \text{ nm}}$ to average $N_{>10 \text{ nm}}$ and the uncertainty of the ratio (σ_R) were derived. New particles are considered to be present when the ratio is above 1.3 plus three times uncertainty as an assumed noise floor:

$$\frac{N_{>3 \text{ nm}}}{N_{>10 \text{ nm}}} > 1.3 + 3 \cdot \sigma_R \quad (1)$$



An NPF event was identified when at least three consecutive 10-s intervals indicate the presence of newly formed particles. Given the P3 flew at ~ 160 m/s, this translates into a minimum spatial scale of ~ 5 km. In total 105 NPF events were identified, and the durations range from 30 to 1150 s, corresponding to spatial scales of 5-196 km.

- 155 To contrast the conditions between NPF events and non-NPF events, we also defined non-NPF periods following a similar approach. Specifically, a non-NPF period consists of a minimum of 6 consecutive 10-s intervals (i.e., a minimum of 60 s in duration) with all intervals during the period showing the ratio of averaged particle concentrations (i.e., $N_{>3\text{ nm}}/N_{>10\text{ nm}}$) statistically below 1.05:

$$\frac{N_{>3\text{ nm}}}{N_{>10\text{ nm}}} < 1.05 - 3 \cdot \sigma_R \quad (2)$$

- 160 We note the criteria for non-NPF periods is quite strict. Due to measurement counting statistics, some of the non-NPF periods might not be identified even though no newly formed particles are present. Similarly, some weak new particle events might not be picked up by the criteria (i.e., Eq. (1)) described above either.

2.3 K-means Classification

- To examine the conditions that lead to NPF, we performed k-means clustering on the matrix consisting of event mean values of aerosol surface area concentration, RH, air temperature, and UV irradiance for 95 NPF events (10 events are excluded due to missing data for one or more of the four variables). RH was included as one of the variables because an elevated RH in the mid to upper FT often indicates air with more moisture and reactive gases (e.g., DMS) that are vertically transported by convective clouds from the lower atmosphere (Reid et al., 2019). The transported reactive gases can be subsequently oxidized to form low volatility species that participate in NPF (Ahern et al., 2019). In addition, elevated water vapor/RH in the cloud outflow regions is typically associated with high concentration of water vapor, which has been shown to participate in binary nucleation (Vehkamäki et al., 2002). The total UV irradiance (i.e., the sum of both upwelling and downwelling components) was included as a proxy for actinic flux due to the absence of direct measurement.

- The four variables (e.g., RH, aerosol particle surface area concentration, air temperature, and UV irradiance) were first normalized using z-score standardization. The optimal number of clusters K was determined as six using the elbow method together with Silhouette coefficient (Syakur et al., 2018; Rousseeuw, 1987). We then performed the k-means clustering via MATLAB based on k-means ++ algorithm (Arthur and Vassilvitskii, 2007; Lloyd, 1982) and a prescribed setting of 5,000 iterations. Consequently, the 95 NPF events were clustered into 6 groups, and each contained 6-30 NPF events. General statistics of six clusters in terms of four key variables are presented in Table 2.

- 180 **Table 2. Mean general statistics of key parameters for the 6 clusters identified using k-means classification.**

Cluster #	Number of events	Total duration, s	Mean altitude, m	Mean temperature, °C	Mean UV irradiance, W m^{-2}	Mean RH, %	Mean surface area, $\mu\text{m}^2 \text{cm}^{-3}$
1	25	4910	7587.6	-14.6	106.1	76.3	4.1



2	14	4320	6480.8	-8.8	60.8	81.9	2.6
3	30	4590	5944.6	-4.4	108.0	77.1	2.9
4	8	1010	7568.2	-14.0	119.6	30.6	4.7
5	12	890	6727.5	-10.3	95.6	62.0	15.6
6	6	400	3959.3	4.2	58.1	74.2	9.5

2.4 Development of Chemical Influence Flag

To investigate the impact of air mass type on NPF, we classified air masses sampled during CAMP²Ex into three types following a similar approach by DiGangi et al (in preparation, also in CAMP²Ex Archive). The flag partitions sources by the observed ratios of enhancement in methane to that in CO ($\Delta\text{CH}_4/\Delta\text{CO}$) through a combination of absolute and correlative methods into 4 regimes: background air (background, hereafter), biomass burning (BB-influenced, hereafter), air mass influenced by urban (urban-influenced, hereafter) and mixed urban/biomass burning. The classification is largely based on $\Delta\text{CH}_4/\Delta\text{CO}$, taking advantage of the relatively long lifetime of both trace gases in the FT. Here the term background is defined to differentiate air masses from the other two types (i.e., impacted by biomass burning or urban emission), which does not strictly refer to very clean conditions. As reported by literature (Nara et al., 2017; Worden et al., 2017), low $\Delta\text{CH}_4/\Delta\text{CO}$ has been frequently observed in biomass burning plumes (typically < 10%), whereas much higher ratios (typically close to 100%) have been reported in fossil fuel combustion emissions (Helfter et al., 2016). In this study, we use these regimes to investigate the impact of air masses on NPF by focusing on NPF events observed in background, biomass burning and urban-influenced air masses.

3 Overall Statistical Analysis

3.1 General Statistics

There was a total of 19 research flights (RFs) during CAMP²Ex. These RFs covered the ocean east and west of Luzon Island, and two of them (RF8 and RF18) sampled over Luzon Island and upwind/downwind of Metro Manila. The date and sampling area of all RFs, together with the duration and key variables of observed NPF events, are presented in Table S1. Most NPF events were observed above 3 km when RH exceeded 50%, and only about 2% of total NPF was observed at 3.5-5 km. A few events were identified within the boundary layer about 50 kilometers downwind west of metro Manila, which are closely associated with shipping and/or urban emissions. These NPF events likely occurred immediately following the dilution of vehicle and engine emissions (e.g., Uhrner et al., 2011; Wehner et al., 2009), and they are not included in further analyses. The number concentration of newly formed particles ($N_{3-10\text{ nm}}$) above 3 km shows large variations among different research flights. NPF frequency, defined as the ratio of the sampling time when new particles were observed to the total flight time, decreased drastically starting from RF11 on 19 September and no events were observed from RF12 through RF17 as shown in Fig. 1.



210 This sudden decrease in NPF frequency coincided with the early monsoon transition starting on 20 September
(Hilario et al., 2021). The impact of the southwest monsoon phase on the occurrence of NPF will be discussed in
Sect. 3.3.

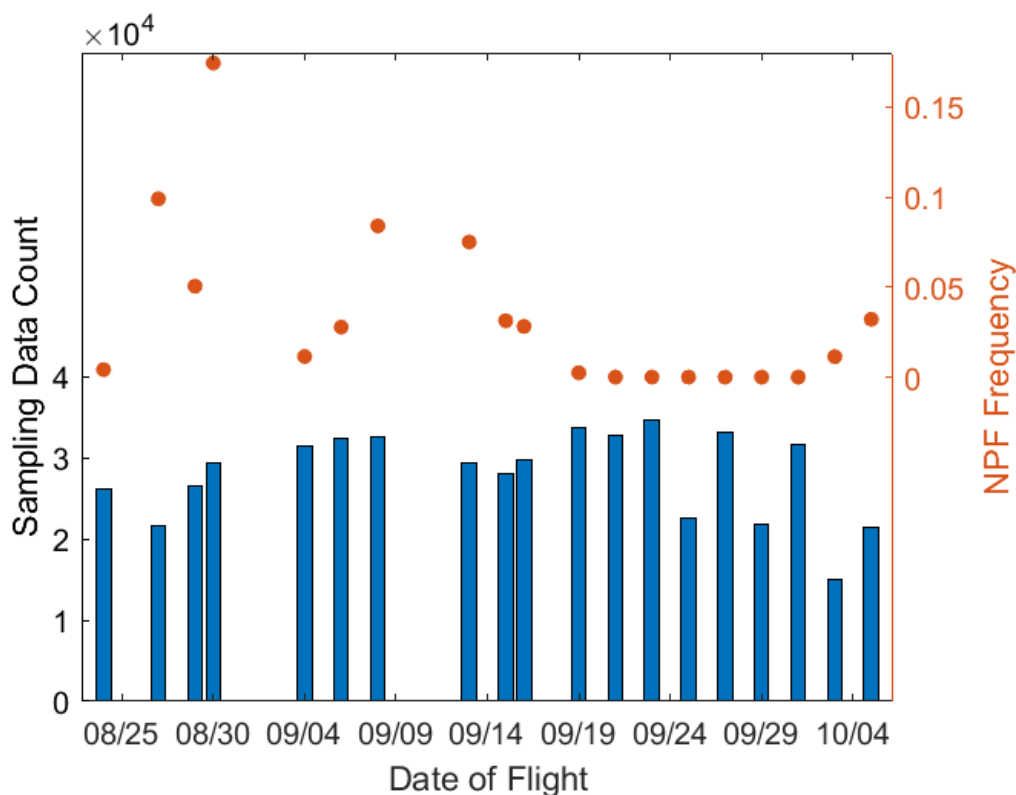


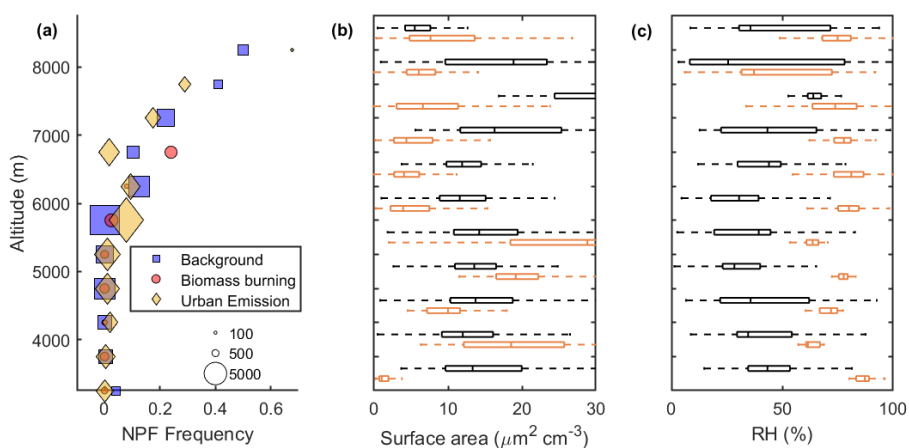
Figure 1. Amount of data sampled during each RF (bars) and corresponding NPF frequency (orange dots), which is defined as the ratio of the duration of NPF events to the total sampling time during the flight.

215 3.2 Dependence of NPF Frequency on Air Mass Types

220 One objective of this study is to investigate the features of NPF and the influence of emission sources on NPF at different altitudes. For each of the three air mass types (i.e., background, urban-influenced, and BB-influenced), NPF frequency is calculated for each 500 m altitude bin. In addition, we compare the vertical profiles of the existing surface area and RH between NPF and non-NPF periods, i.e., periods when newly formed particles were observed and absent, respectively (see Sect. 2.2 for the definitions of NPF and non-NPF periods). Note that due to the limited sampling, no non-NPF periods above 7.5 km are identified based on the criteria described in Sect. 2.2. For the comparison above 7.5 km, the non-NPF period is instead defined as the entire period when P3-B sampled outside clouds except when newly formed particles were observed (i.e., when Eq. (1) is satisfied).



225 Figure 2a shows that below 5.5 km, no NPF events were observed in background or BB-influenced air masses and NPF frequency is very low (below 3%) in the air influenced by urban emissions. NPF frequency shows strong increases with altitude above 6 km for all three air mass types, reaching about 49% above 8 km. Figure 2c shows that over the entire altitude ranges examined, NPF consistently occurred in air with elevated RH. This suggests NPF in outflow regions and detrainment layers of convective clouds, which is confirmed by the flight video, is also consistent with earlier studies (Clarke et al., 1998; Perry and Hobbs, 1994). However, the impact of surface area on NPF shows an altitude dependence (Fig. 2b). Above 5.5 km, newly formed particles were observed when surface area was reduced, generally consistent with the higher NPF frequency in background airmass. In contrast, NPF coincided with relatively high surface area below 5.5 km, where all NPF events were observed in urban influenced airmasses. The altitude dependence of the impact of airmass and surface area on NPF implies the competing influences from different processes (i.e., production and removal of nucleating species) that varies with altitude, 235 which will be further discussed in Sect. 4.



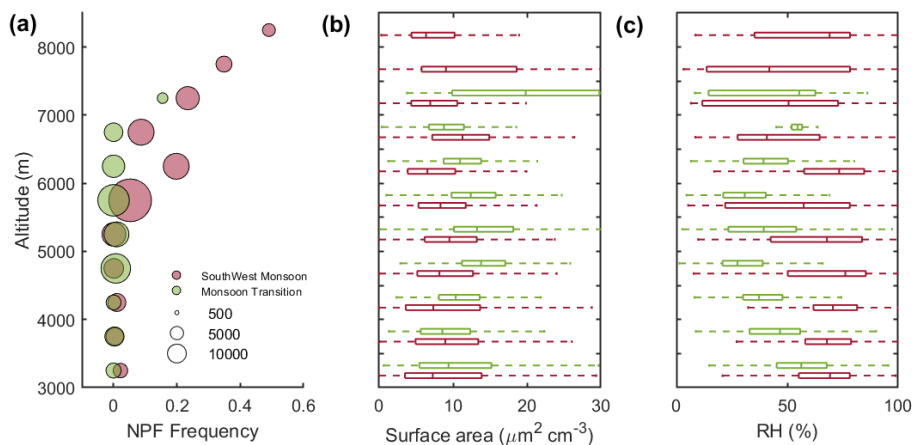
240 **Figure 2.** (a) The vertical profile of NPF frequency for the three air mass types. NPF Frequency is defined as the ratio of total duration of NPF period to the total sampling time outside of the clouds for each airmass type. Also shown are the comparison of (b) surface area and (c) relative humidity (RH) between NPF and non-NPF periods, where black denotes non-NPF and orange denotes NPF.

3.3 Impact of Monsoon Transition on NPF Frequency

245 As shown in Fig. 1, the NPF frequency during the southwest monsoon (SWM; RF1-11) with its Maritime Continent source region was much higher than that during the Monsoon transition/post monsoon phase (MT; RF12-19). The reduction of NPF frequency occurs at all altitudes above 5.5 km during the MT. The RH was higher during SWM compared to that during MT over most altitudes above 3 km (Fig. 3c), whereas the surface area was generally lower during SWM (Fig. 3b). These differences suggest that lower NPF frequency during the MT is due to, at least partially, the higher surface area (larger condensation and coagulation sinks), which is likely a result of less convective activity and thus reduced precipitation that would remove existing particles. The more frequent long-



250 range transport of aged pollution from East Asia may also contribute to the higher surface area during the MT (Hilario et al., 2021).



255 **Figure 3. Comparison of vertical profiles between SouthWest Monsoon (SWM; 24 August to 20 September) and Monsoon Transition (MT; 20 September to 5 October) regarding frequency of new particle formation (a), surface area (b) and RH (c). The size of circles denotes the amount of data sampled in the corresponding altitude bin.**

3.4 K-means Classification Results

As described in Sect. 2, a total number of 95 NPF events were classified into six clusters based on RH, temperature, UV irradiance and surface area. Figure 4 shows the contributions of air mass types to each cluster as well as the statistical comparison of key variables during NPF events of each cluster and those during corresponding non-NPF events. For each NPF event cluster, the corresponding non-NPF events are defined as the periods when no newly formed particles were observed based on Eq. (2) within the same altitude range of the NPF events. This is to minimize the impact of altitude, as the NPF frequency strongly depends on the altitude (Fig. 2a).

265 Figure 4a shows the contribution of different air mass types to each NPF event cluster and the mean altitudes for the clusters. Clusters #1-3 represent the vast majority (i.e., 76%) of data collected during the NPF events. NPF events in cluster #1 and #2 were mostly observed in background air, with a small portion in urban-influenced air masses. In contrast, cluster #3 consists mostly of polluted air masses (i.e., BB-influenced or urban-influenced). Altogether, clusters #4-6 represent 24% of the NPF event data, the majority of which was in urban-influenced air masses. Figure 4b-f show that new particles form under a wide range of conditions, and the formation exhibits varying intensities, as suggested by different $N_{3-10\text{ nm}}$ values. Most of the NPF events were observed in air masses with surface area below $10\ \mu\text{m}^2\ \text{cm}^{-3}$, in good agreement with findings from earlier studies (Clarke et al., 1999). However, NPF events in cluster #5 occurred when SA was elevated compared to that during non-NPF periods at similar altitudes. These NPF events included in cluster #5 were mostly observed during RF18 and RF19, and part of this cluster corresponds



to the NPF events with higher surface area below 5.5 km shown in Fig. 2b. The potential mechanism for such NPF events will be discussed in Sect. 4.3. Figure 4b shows that most of NPF occurred with high actinic flux (indicated indirectly by the UV irradiance data during this campaign), as in clusters 1, 3, and 5. However, cluster #2 NPF events occurred with much lower UV irradiance level and surface area, which will be discussed later in Sect. 4.1. In terms of RH, except for cluster #4, all NPF clusters were observed with median RH above 50% and the RH is statistically higher than that during corresponding non-NPF events, again indicating that NPF mostly takes place in air masses processed by convective clouds. NPF in cluster #4 occurred under the driest conditions (Fig. 4f) but with the highest UV irradiance (Fig. 4b), and $N_{3-10\text{ nm}}$ is statistically the lowest among all clusters (Fig. 4e).

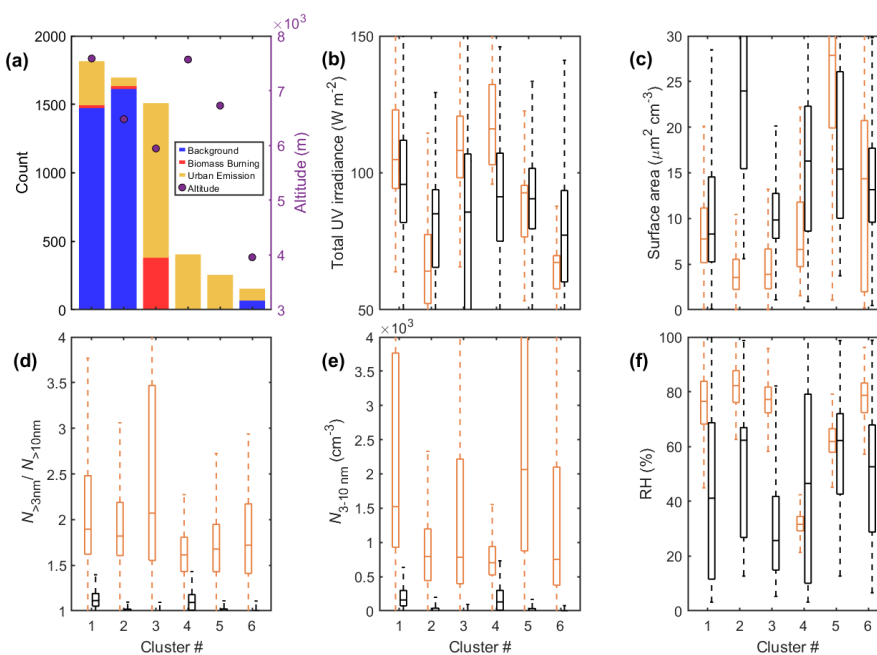


Figure 4. (a) Number of 1-s data classified into each cluster and contributions of different air mass types. The other five panels compare NPF events of each cluster and corresponding non-NPF periods at the same altitude ranges in terms of (b) total UV irradiance, (c) existing aerosol surface area, (d) the ratio of number concentration of particle larger than 3 nm to that of particle larger than 10 nm, $N_{>3\text{ nm}}/N_{>10\text{ nm}}$, (e) number concentration of particles in diameter range of 3–10 nm, $N_{3-10\text{ nm}}$, (f) RH.

4 Characteristics of NPF in Different Air Mass Types

Here, we combine the k-means classification (i.e., based on T, RH, surface area concentration and UV irradiance) and air mass classification to investigate the impact of both meteorological conditions and emissions on NPF. We divide the above clusters into multiple types, including NPF in background, mid-altitude NPF in polluted air, high-



altitude NPF in polluted air, etc. In the following sections, we will examine NPF of each type and investigate the conditions that lead to NPF for different air masses as a function of altitude.

4.1 NPF Observed in Background Air

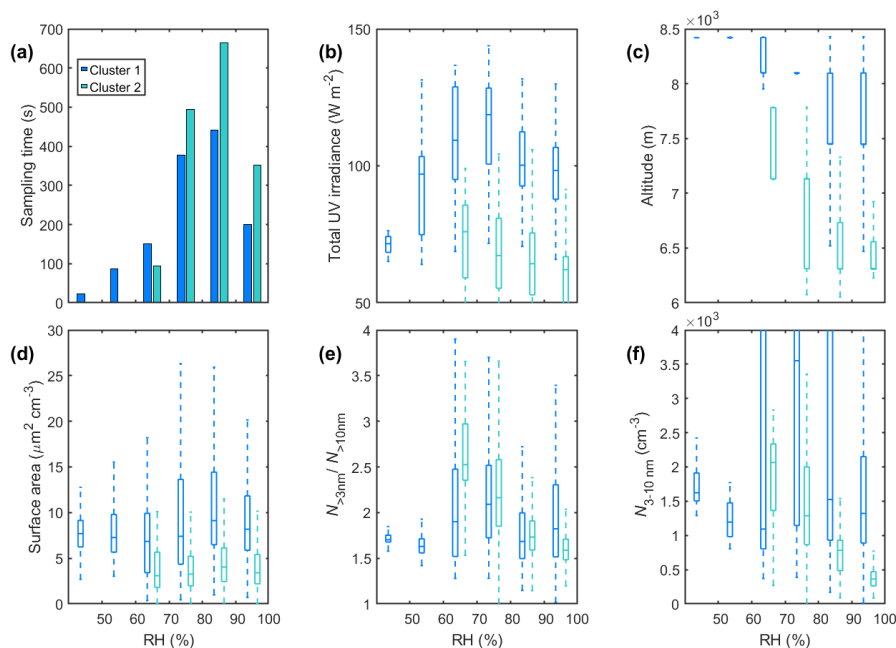
295 NPF in background air (CO concentration < 110 ppbv and CH₄ concentration < 1.86 ppm) was mostly observed in the early part of the campaign (i.e., RF2-6) during the southwest monsoon phase. These NPF events, mostly classified as clusters #1 and #2 (Fig. 4a), took place from 6 km up to 8.5 km over Sulu Sea/West Luzon. General features of these events (background NPF, hereafter) are high RH and low surface area, indicating new particles were formed in air processed by convective clouds.

300 We further divided background NPF events into two types based on the result of k-means classification: one classified into cluster #1 (mostly sampled during RF4 and RF6) while the other classified into cluster #2. The main differences between these types include UV irradiance (Fig. 5b), altitude (Fig. 5c), and surface area (Fig. 5d). Figure 5 compares two types of background NPF in terms of data number distribution as well as key statistics as a function of RH. For both types, RHs are mostly in the range of 60-100% and concentrated between 70% and 90%. The high

305 RH indicates that both types of NPF took place in cloud processed air (e.g., outflow region or detrainment layers). UV irradiance, $N_{>3\text{ nm}}/N_{>10\text{ nm}}$, and $N_{3-10\text{ nm}}$ show similar variations with RH (Fig. 5b, e, and f), and exhibit the highest values in the RH range of 60-80%. This suggests UV irradiance plays an important role in these background NPF events, in agreement with the earliest findings of Perry and Hobbs (1994). The enhanced irradiance is attributed to the presence of clouds, as confirmed from the recorded videos by the forward camera onboard the P-3B. The effect

310 of UV irradiance on NPF is also consistent with an earlier study (Wehner et al., 2015) that shows newly formed particles in regions with enhanced UV irradiance near cumulus clouds. The UV irradiance decreases from the peak values as RH increases above 80% and approaches 100%, accompanied by decreases in $N_{>3\text{ nm}}/N_{>10\text{ nm}}$ and $N_{3-10\text{ nm}}$. The decrease in UV irradiance above 80% RH is likely due to attenuation of solar radiation in the immediate vicinity of clouds and between cloud layers (Hamed et al., 2011). In addition, it takes some time for the incipient particles to

315 grow and reach detectable sizes (i.e., > 3 nm). Therefore, the reduced $N_{>3\text{ nm}}/N_{>10\text{ nm}}$ and $N_{3-10\text{ nm}}$ when RH is above 80% are likely due to a combination of reduced actinic flux and recently nucleated particles having not reached detectable sizes yet in the immediate vicinity of clouds.



320 **Figure 5. (a) Sampling time, (b) UV irradiance, (c) altitude, (d) surface area, (e) $N_{>3\text{ nm}}/N_{>10\text{ nm}}$ and (f) $N_{3-10\text{ nm}}$ as function of RH for two types of background NPF classified as cluster #1 and #2, respectively.**

Whereas the two background NPF types share many similar features, there are also clear differences between them. The background NPF with low UV irradiance was mostly observed in the early morning, whereas in previous studies NPF was often observed later in the day when solar radiation is strong. We note that under clear sky, UV actinic flux has a weaker dependence on solar zenith angle (SZA). The UV actinic flux is estimated from the UV irradiance, SZA, and cloud condition (Details in SI). Both UV irradiance and actinic flux during the morning background NPF events are statistically lower than those during the NPF events that occurred during 10:00-14:00 in the same altitude range (Fig. S2). The median UV irradiance during morning NPF events is about 28% lower than that of the NPF events around noon, while the median UV actinic flux is about 11% lower.

One possible explanation is that these new particles were formed during the previous daytime under high UV irradiance/actinic flux, survived scavenging overnight and were detected the next morning. In such a scenario, it is expected that the existing particle surface area at the time of NPF should be similar or even lower than the surface area when the new particles were observed the next morning. This is because if the surface area was reduced by wet scavenging after NPF, the newly formed particles would have been efficiently removed by coagulation with large cloud droplets, and no NPF events would be identified the next morning. Because there are no continuous measurements from late afternoon to the next morning, we statistically compare the total sampling time and the NPF frequency between early morning (7:00-10:00 local time) and late afternoon (15:00-18:00 local time) above 5 km



during the whole mission, and the results are shown in Fig. 6. During CAMP²Ex, measurement periods above 5 km and after 15:00 local time are much shorter than those during 7:00-10:00. The percentage of the data with surface area below $5 \mu\text{m}^2 \text{cm}^{-3}$ in the early morning (i.e., 7:00-10:00) is about 22%, significantly higher than that in the late afternoon (4%, 15:00-18:00), indicating the condition of low surface area is much more prevalent during the early morning. In addition, the frequency of NPF in the early morning is about 20 times higher than that in the afternoon, suggesting that new particles observed were most likely formed in the morning, instead of the day before. Otherwise, the frequency of NPF in the afternoon would have exceeded or at least be comparable to that in the early morning. The NPF in the early morning is likely made possible by the much lower surface area (i.e., condensation sink for the nucleating species), despite the lower UV irradiance and actinic flux compared to the non-NPF periods at same altitudes. We speculate the prevalence of low surface area in the early morning is due to a combination of wet scavenging and less convection (i.e., reduced vertical transport of aerosol particles from near the surface to the FT) overnight. It is worth noting that nighttime NPF has been reported in conditions of low surface area in the upper FT (Lee et al., 2008). However, the mechanism of nocturnal NPF is not well understood. Given the absence of nighttime measurements during the campaign, we cannot exclude the possibility that some of the new particles observed in the early morning were formed during the nighttime.

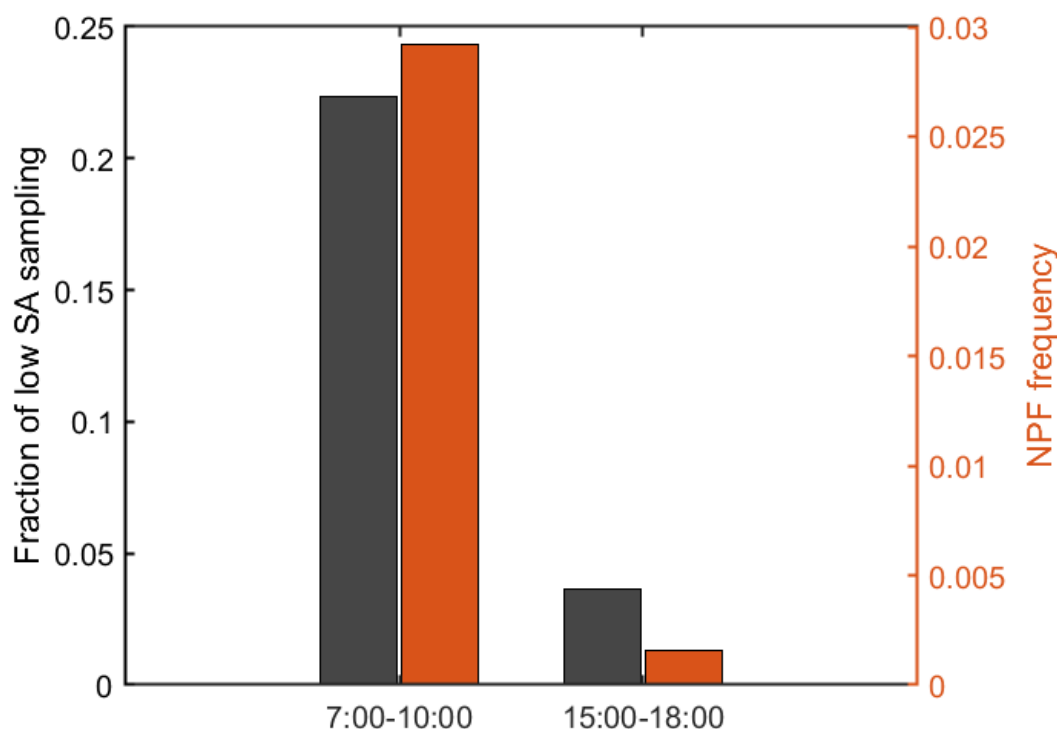




Figure 6. Comparison of the fraction of outside of cloud sampling in low surface area condition (the ratio of amount of data with surface area lower than $5 \mu\text{m}^2 \text{cm}^{-3}$ to total sampling time in the early morning or late afternoon, black bars) and NPF frequency (the ratio of sum of NPF events to total sampling time, orange bars) between early morning (7:00-10:00) and late afternoon (15:00-18:00).

4.2 NPF Associated with Biomass Burning Smoke

Biomass burning is one of the major aerosol sources, emitting not only a large amount of primary particles but also precursors such as SO_2 (Crutzen and Andreae, 1990), DMS (Meinardi et al., 2003) and organic gases that lead to secondary aerosol formation (Hennigan et al., 2012; Spracklen et al., 2011; Fiedler et al., 2011; Meinardi et al., 2003). Few direct measurements of NPF in biomass burning plumes have been reported (Shang et al., 2018; Vakkari et al., 2018; Hodshire et al., 2021). Biomass burning smoke originating from the Borneo region was sampled during the research flight on 15 September (RF9), during which high $N_{3-10 \text{ nm}}$ was observed together with a strongly enhanced CO mixing ratio (ΔCO) that is 3-5 times above typical values in background or urban-influenced air masses. The NPF events in BB-influenced air mass were observed at 6.7 km. A HYSPLIT-based five-day backward trajectory analysis was simulated using similar methods to a previous measurement report (Hilario et al., 2021) for air masses arriving at different sampling altitudes of RF9 on 15 September 2019. Within the boundary layer, the prevailing wind was from the southwest and air masses originated from Borneo regions, where strong biomass burning activities were reported. In contrast, air masses arriving at 6.7 km came from the west Pacific with no direct influence by biomass burning (Fig. S3). The BB-influenced air mass observed in the FT during RF9 is therefore due to the vertical lifting and detrainment of the biomass burning plume by convective clouds, instead of direct long-range transport inside the FT from Borneo. The biomass burning plume had travelled inside the boundary layer across the Sulu Sea from the Borneo (Fig. S3), consistent with previous findings that transport of smoke to the region mostly occurred within boundary layer due to strong wind shear during the southwest Monsoon season (Hilario et al., 2020; Xian et al., 2013).

To investigate the potential impact of biomass burning emissions on NPF, we compare NPF observed during RF9 to background NPF from other flights within the same altitude range. Because no measurements of non-methane hydrocarbons are available during CAMP²Ex, we use CO as a surrogate for VOCs emitted from biomass burning. As UV irradiance plays an important role in NPF, the key variables including $N_{>3 \text{ nm}}/N_{>10 \text{ nm}}$ and $N_{3-10 \text{ nm}}$ during both BB-influenced and background NPF events are compared for the same UV irradiance levels (Fig. 7).

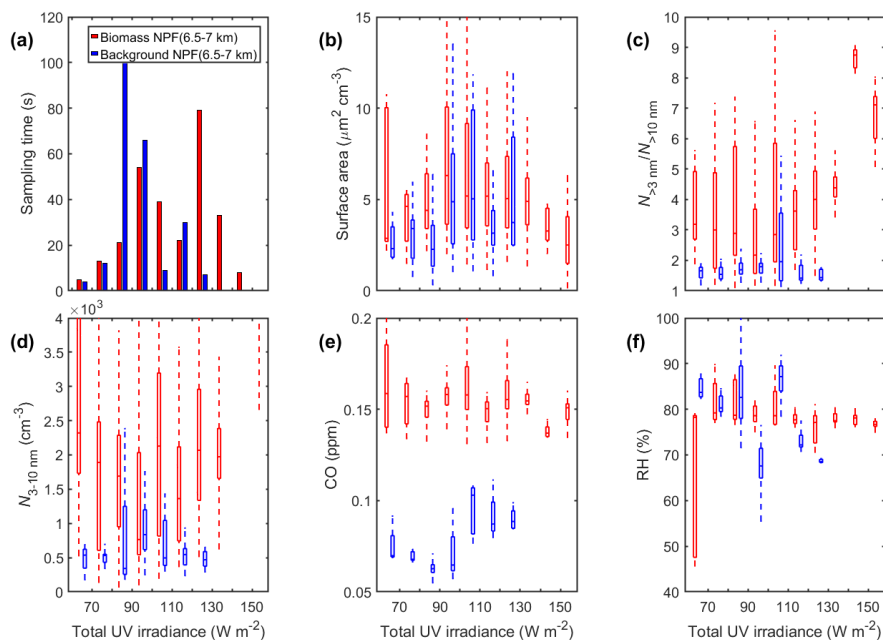


Figure 7. Comparison between NPF influenced by biomass burning smoke and NPF in background. (a) Sampling time, (b) surface area, (c) $N_{>3 \text{ nm}}/N_{>10 \text{ nm}}$, (d) $N_{3-10 \text{ nm}}$, (e) CO and (f) RH are plotted as a function of UV irradiance.

385

We focus on the comparison for UV irradiance ranging from 70–130 W m^{-2} based on background NPF such that data sizes for both NPF types are comparable. There exists a substantial fraction of BB-influenced NPF with UV irradiance higher than 130 W m^{-2} , whereas few non-BB NPF events at the same altitude range had UV irradiance above 130 W m^{-2} . For the same UV irradiance level, BB-influenced NPF occurred with similar or slightly higher surface area compared to the background NPF (Fig. 7b) but with much stronger intensity (i.e., $N_{>3 \text{ nm}}/N_{>10 \text{ nm}}$ and $N_{3-10 \text{ nm}}$, Fig. 7c, 7d). The stronger NPF in the BB-influenced airmass at the same UV irradiance level and similar or slightly higher surface area indicates that precursors emitted by biomass burning enhances NPF, as indicated by elevated CO mixing ratio (Fig. 7e). The similar or only slightly higher surface area of BB-influenced NPF events suggests that the existing particles were efficiently removed through wet scavenging as the biomass burning plume was lifted into the FT by the convective clouds. Despite a high concentration of precursors, the efficient removal of existing particles appears to be a necessary condition for NPF to occur in the aged BB-influenced air masses. There are two leveled flight segments at the same altitude of 6.7 km during RF9. NPF was observed during one segment with much reduced surface area and non-volatile particle concentration. For the other segment, the concentrations of non-volatile particles and larger particles ($> 100 \text{ nm}$) were three times as high as when NPF was absent (Fig. S4). It remains unclear which nucleation pathway dominates particle formation observed in BB-influenced air mass, since organic vapors, ammonia (Hegg et al., 1988) and sulfuric acid can directly or indirectly originate from biomass

390

395

400



burning plumes and contribute to formation of secondary aerosols (Ahern et al., 2019). In terms of potential organic precursors, oxygenated aromatics together with heterocyclic compounds were reported to account for almost 80% of total mass of secondary aerosols (Akherati et al., 2020). Other laboratory studies reported that oxidized aromatic VOCs such as benzenediols, phenols and benzaldehyde were dominant potential precursors (Gilman et al., 2015; Yee et al., 2013). More measurements are required to investigate nucleation mechanisms in air masses influenced by biomass burning plumes and the potential impact of aging and scavenging during long-range transport.

405

4.3 NPF Influenced by Urban Emissions

Besides background and BB-influenced NPF, NPF events were also observed in many air masses influenced by urban emissions. These urban-influenced NPF events exhibit quite different conditions, (e.g., RH, surface area), and are classified into different k-means clusters. Therefore, the discussion of NPF in air masses influenced by urban emissions (urban influenced NPF, hereafter) will follow the classification by k-means clustering (see Fig. 4). A large fraction of cluster #3 is classified as urban-influenced, which is mostly from RF7 and RF8 at an altitude of 5.5-6.5 km, while a small fraction of cluster #1 and entire cluster #4 represent urban influenced NPF at altitudes above 7 km. The remaining are distributed throughout cluster #5-6 and exhibit contrasting features, i.e., occurring with elevated surface area compared to the non-NPF periods at comparable altitudes (Fig. 4c).

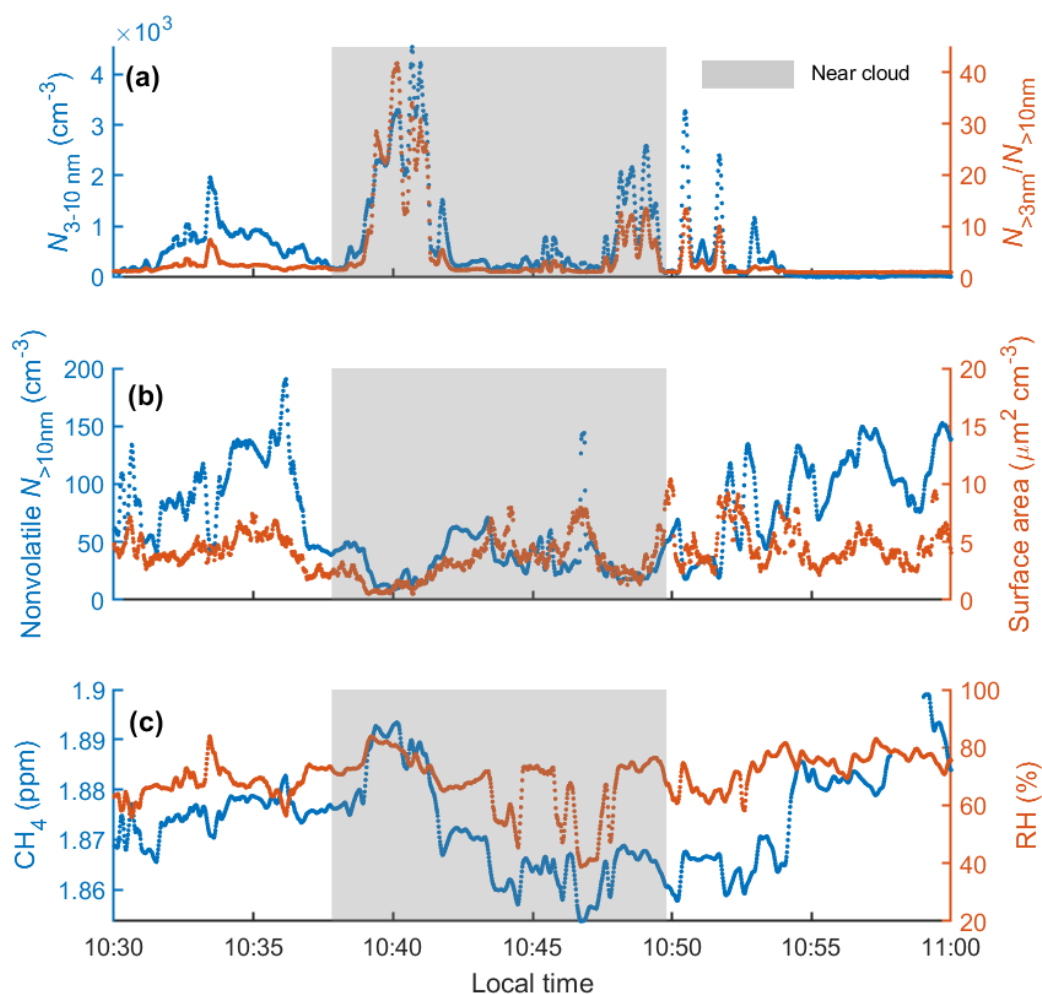
410

415

4.3.1 NPF over Coastal Regions and Land at Altitudes of 5.5-6.5 km

Urban influenced NPF classified as cluster #3 shares some similar features with the NPF observed in BB-influenced airmasses. The locations of these urban influenced NPF events are shown in Fig. S5. Measurements on 13 September 2019 show elevated $N_{>3\text{ nm}}/N_{>10\text{ nm}}$ and $N_{3-10\text{ nm}}$ during the level flight near Manila. In addition, on 8 September 2019, extremely high $N_{>3\text{ nm}}/N_{>10\text{ nm}}$ values up to 40 and $N_{3-10\text{ nm}}$ above 4000 cm^{-3} were observed at altitudes of ~ 6.3 km over the West Pacific about 50 km away from the coastline. These events together represent over 80% of data classified as cluster #3, and the general features include low surface area, high UV irradiance and high RH, similar to BB-influenced NPF events.

420



425

Figure 8. Time series plot for a segment with NPF observed in an urban emission influenced air mass near cumulus clouds during RF7 (8 September 2019), including (a) $N_{3-10 \text{ nm}}$ and $N_{>3 \text{ nm}}/N_{>10 \text{ nm}}$, (b) number concentration of non-volatile particles larger than 10 nm and surface area, and (c) CH_4 mixing ratio and RH.

Figure 8 shows the key variables during a representative urban-influenced NPF event, which was observed over the ocean east of Luzon during RF7. The time series shows drastically increased $N_{>3 \text{ nm}}/N_{>10 \text{ nm}}$ and elevated CH_4 concentration around 10:40, which were observed near convective clouds based on video from the forward-looking camera. Starting from $\sim 10:35$, both the surface area and concentration of non-volatile particles (nonvolatile $N_{>10 \text{ nm}}$) decrease, while RH and CH_4 concentration become elevated, indicating the uplift of humid and urban influenced air from lower altitude. The concurrence of drastically increased $N_{>3 \text{ nm}}/N_{>10 \text{ nm}}$ and elevated CH_4 suggests trace gases

430



435 emitted in urban areas contribute to the production of nucleating species and NPF. Here CH₄ is used as a surrogate
for emitted precursors in urban plumes, which typically include SO₂, gaseous sulfuric acid and organic species
(Zhang et al., 2012). A positive correlation between $N_{>3\text{ nm}}/N_{>10\text{ nm}}$ and CH₄ concentration is also found during the
leveled box flight segment of RF8, which took place close to Manila (not shown). Compared to most other NPF
events, these events were observed closer to urban areas over the land and are therefore more likely influenced by
440 fresh urban emissions.

Given the dependence of NPF on multiple parameters (e.g., surface area, UV irradiance, and precursor
concentrations), the potential impact of urban emissions on NPF is examined statistically. One approach is to
statistically compare $N_{>3\text{ nm}}/N_{>10\text{ nm}}$ and $N_{3-10\text{ nm}}$ between urban-influenced NPF (i.e., classified in cluster #3) and
background NPF events under same conditions (i.e., altitude, surface area, RH, and UV irradiance). However, such
445 comparison is not possible as most background NPF events observed at similar altitudes had substantially lower UV
irradiance (below 100 W m⁻², cluster #2). As a result, the impact of urban emission on NPF was examined by
statistically comparing urban influenced NPF and non NPF events at the similar altitude range and time of the day
(i.e., solar radiation) as a function of surface area. Figure 9 shows that urban influenced NPF occurred mostly with
surface area less than ~6 μm² cm⁻³, substantially lower than during most of the non-NPF periods. For surface areas
450 below 6 μm² cm⁻³, the UV irradiance and RH are statistically similar between urban influenced NPF events and non-
NPF periods, whereas urban influenced NPF events show elevated CH₄ concentration. This suggests that precursors
emitted from urban areas likely contribute to the formation of nucleating species and NPF.

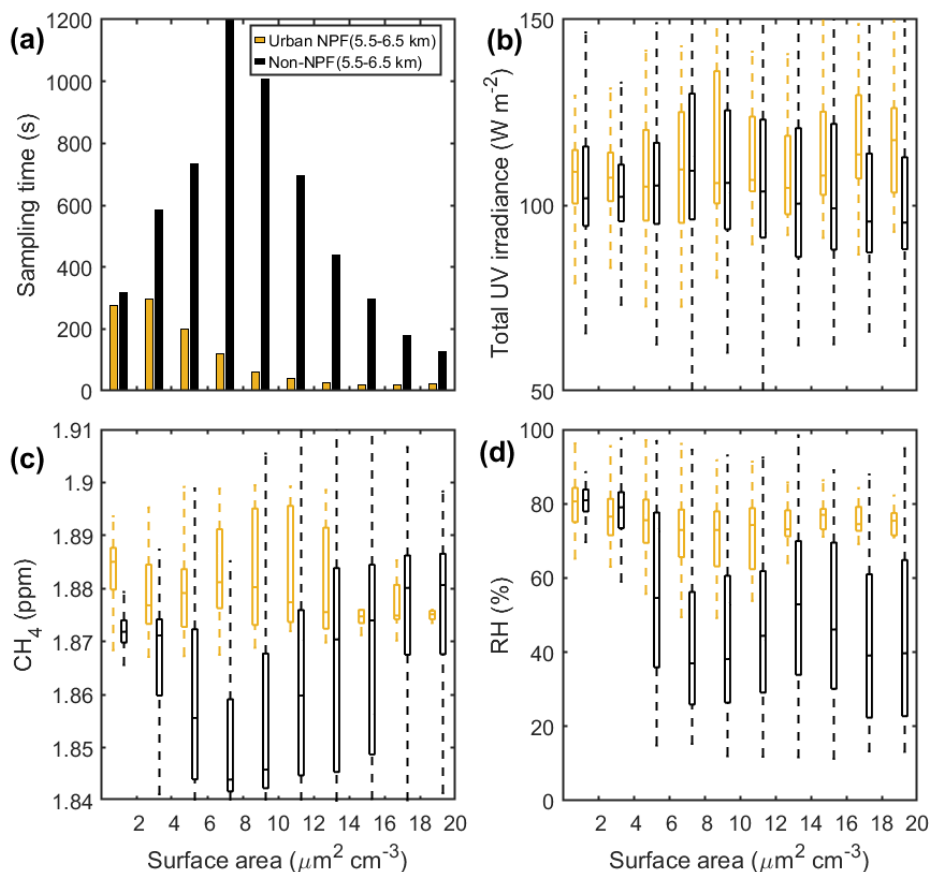


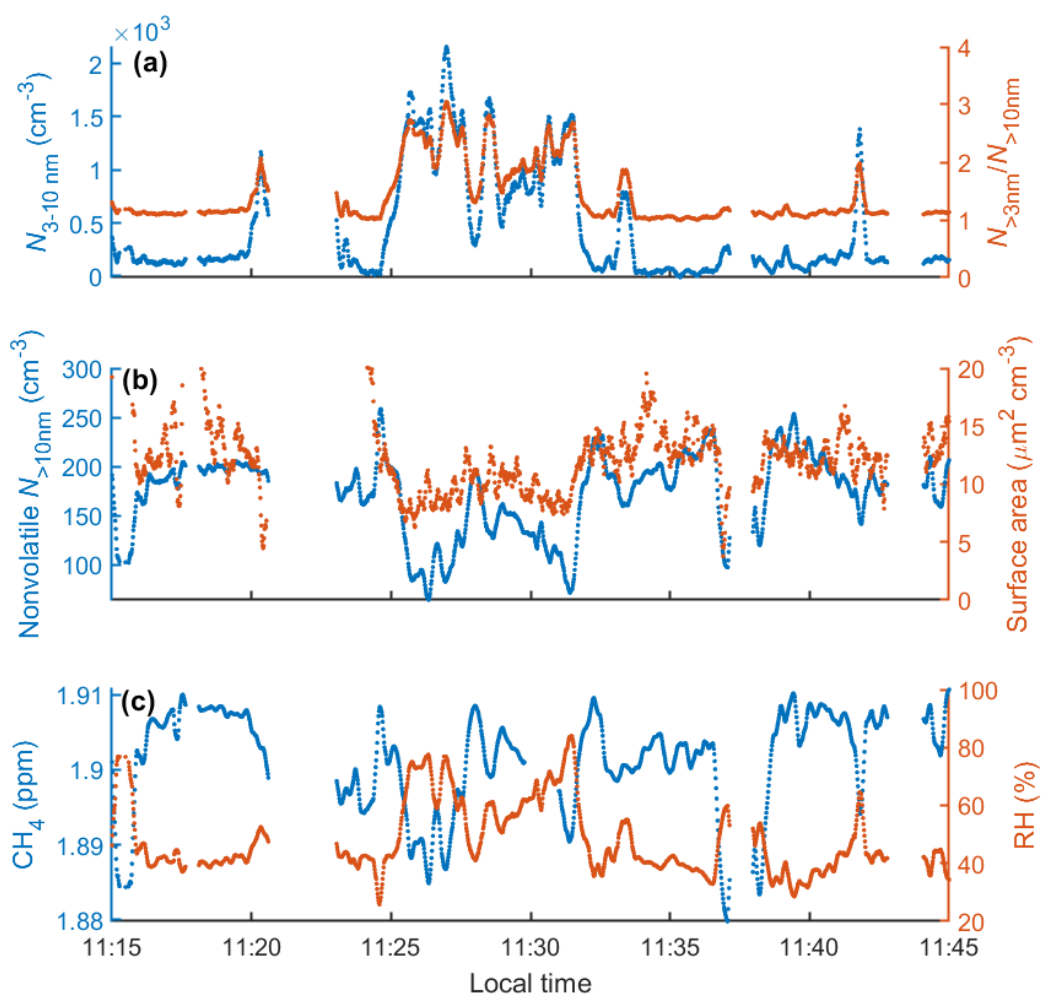
Figure 9. (a) Sampling time, (b) UV irradiance, (c) CH_4 and (d) RH as function of surface area for urban
 455 influenced NPF events at 5.5-6.5 km (yellow) and non-NPF data (black) at same altitude and time range
 (considering the dependence of UV irradiance on altitude).

4.3.2 NPF Influenced by Aged Urban Plume

Part of cluster #1 and #4 represent urban-influenced NPF observed at higher altitudes (~ 7 -8.1 km) than urban-
 influenced NPF observed between 5.5 and 6.5 km. In addition to the difference in altitude range, these NPF events
 460 were observed over the ocean and exhibit relatively lower RH (below 50%) and higher surface area (above $10 \mu\text{m}^2$
 cm^{-3}). Figure 10 shows representative examples of such NPF events, which were observed during RF10 over the
 west Pacific and 600 km away from the coast. During the NPF events $N_{>3 \text{ nm}}/N_{>10 \text{ nm}}$ and $N_{3-10 \text{ nm}}$ reached 3 and 2000
 cm^{-3} , respectively. The elevated $N_{>3 \text{ nm}}/N_{>10 \text{ nm}}$ and $N_{3-10 \text{ nm}}$ coincide with elevated RH and reduced surface area (Fig.
 10a-c), and both $N_{>3 \text{ nm}}/N_{>10 \text{ nm}}$ and RH are anti-correlated with CH_4 concentration during the period (Fig. 10a, 10c),



465 indicating particle formation in cloud outflow regions with reduced CH₄ concentration. Back-trajectories and
elevated CH₄ level (i.e., around 1.9 ppm) suggest the air mass at the sampling altitude was influenced by aged urban
plumes transported from East Asia. The anti-correlations between RH and CH₄ indicate that humid background (i.e.,
low CH₄ concentration) air was lifted by convective clouds and mixed into the aged urban plume. We expect the
reactive precursors in the aged urban plume were mostly consumed during the long-range transport, while CH₄
470 concentration and existing particle surface area remain relatively high due to longer lifetimes in the FT. As a result,
NPF only occurs when the aged plume is mixed with sufficient air detrained from convective clouds, which is
expected to have reduced surface area and elevated concentration of reactive gases such as DMS. Therefore, the
aged urban plume tends to suppress NPF instead of promoting it, as in air masses influenced by fresh urban
emissions shown in Sect. 4.3.1.



475

Figure 10. Time series plot of a level flight segment from RF10 (16 September 2019) where NPF was observed, including (a) $N_{3-10 \text{ nm}}$ and $N_{>3 \text{ nm}}/N_{>10 \text{ nm}}$, (b) number concentration of non-volatile particles larger than 10 nm and surface area, and (c) CH_4 mixing ratio and RH.

4.3.3 Urban Influenced NPF with High Surface Area

480 Unlike most NPF events during CAMP²Ex, a small fraction of urban influenced NPF events occurred with high surface area. These events were grouped into different clusters (i.e., clusters #5 and #6) by the k-means clustering method. Figure 11 shows increasing $N_{3-10 \text{ nm}}$ with concentration of accumulation mode particles (i.e., $N_{>100 \text{ nm}}$) during some examples of such NPF events. These examples were observed at 4.8 km ($\sim 0^\circ\text{C}$) over Metro Manila during



RF18, which was designed to sample urban plumes from Metro Manila. As new particles are typically formed when
485 the concentration of existing large particles is low, a negative correlation between $N_{3-10\text{ nm}}$ and $N_{>100\text{ nm}}$ is expected.
The positive correlation, together with the sampling location, suggests that both $N_{3-10\text{ nm}}$ and the accumulation mode
particles might originate from primary emissions in Metro Manila. Previous studies show that aerosol particles with
diameters of a few nanometers can form as the fresh exhaust from diesel/gasoline engines rapidly cools. While these
nanoparticles are formed through nucleation, they are often considered “primary” as the nucleation process occurs
490 very close to the sources (Uhmer et al., 2011; Wehner et al., 2009). If the elevated $N_{3-10\text{ nm}}$ was due to primary
emissions in metro Manila, we would expect even higher $N_{3-10\text{ nm}}$ at lower altitudes. However, no NPF events were
identified when P-3B sampled in the metro Manila regions below 4.8 km. In addition, albeit from a different flight,
the vertical profiles of aerosol and trace gases during a descending leg over Lingayen Gulf (RF8, Fig. 12) show that
the small particles with diameters between 3 and 10 nm are secondary despite a positive correlation between $N_{3-10\text{ nm}}$
495 and $N_{>100\text{ nm}}$. The vertical profiles show several detrainment layers with elevated $N_{3-10\text{ nm}}$ from 2.5 km up to 4.5 km,
whereas the small particles were mostly absent below 2.5 km. It is worth noting that only the segment of 4–4.5 km
was identified as an NPF event due to its sufficiently long duration (i.e., more than 30 seconds). In individual
detrainment layers, surface area, CO, and CH₄ are locally enhanced, and $N_{3-10\text{ nm}}$ can be positively correlated with
 $N_{>100\text{ nm}}$ as observed in the layer around 3.4 km. However, the comparisons among the different layers show that $N_{3-10\text{ nm}}$
500 increases while $N_{>100\text{ nm}}$, surface area, and CO decrease with altitude, indicating the observed small particles
were formed in the detrainment layers instead of originating from the primary emissions near the surface. The
mechanism for this type of NPF is likely similar to those observed in polluted urban boundary layers (Alam et al.,
2003; Zhu et al., 2014), where high concentrations of precursors make nucleation and particle formation possible
despite relatively high condensation sink conditions. The absence of NPF below 2 km suggest the scavenging of
505 existing particles, while not as pronounced as during the NPF events observed at higher altitudes (e.g., >6 km), still
plays an important role in NPF in these detrainment layers below 5 km.

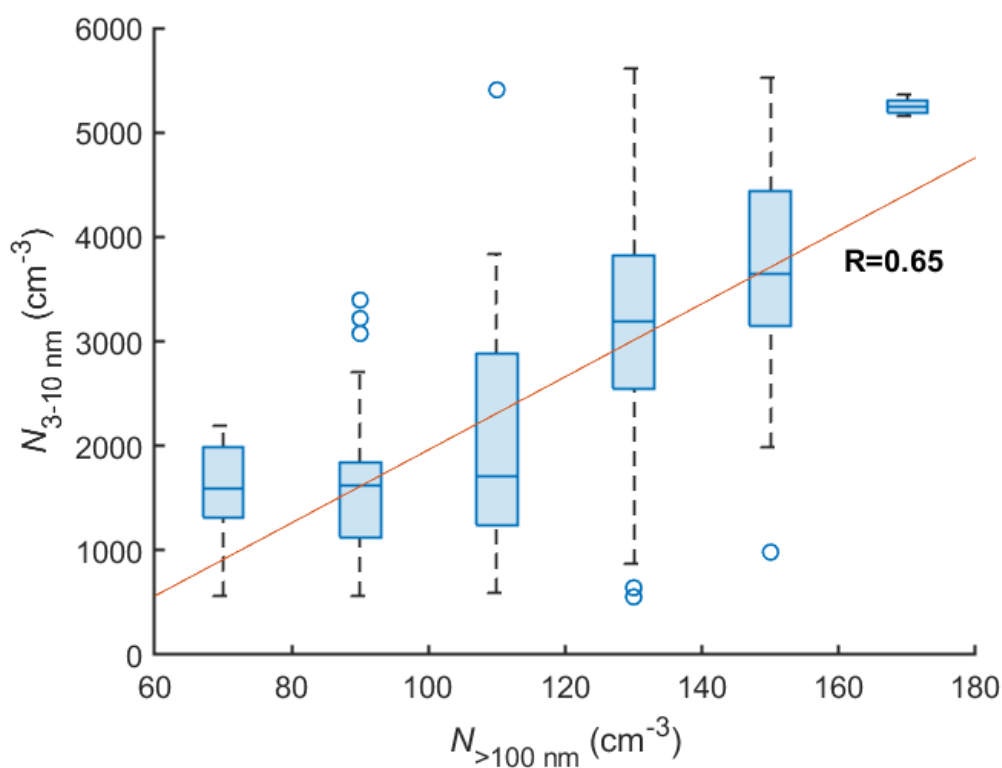


Figure 11. Box whisker plots of $N_{3-10 \text{ nm}}$ for different $N_{>100 \text{ nm}}$ bins during the NPF event observed during RF18 (3 October 2019) over Metro Manila. The $N_{>100 \text{ nm}}$ bins have a width of 20 cm^{-3} (i.e., $60\text{-}80 \text{ cm}^{-3}$, $80\text{-}100 \text{ cm}^{-3}$..., 160-1180 cm^{-3}). Orange line represents a linear fit of all 170 individual data points ($R=0.65$).

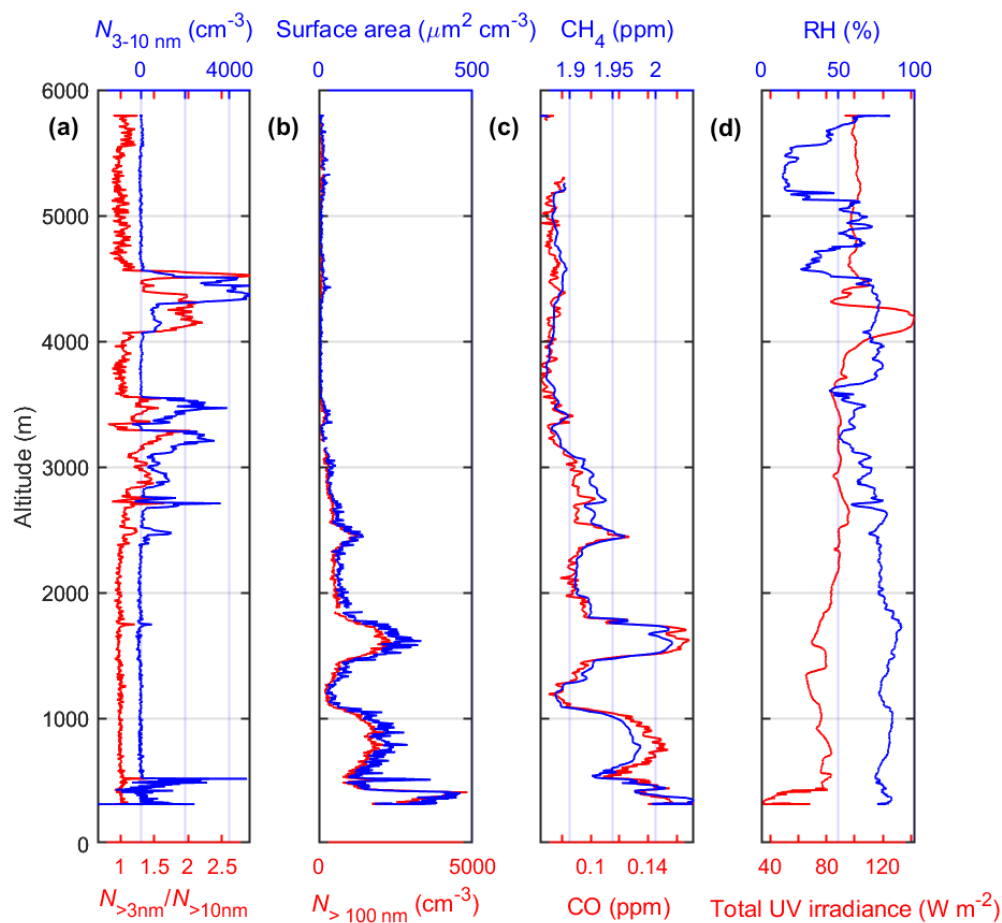


Figure 12. Vertical profiles of (a) $N_{>3 \text{ nm}}/N_{>10 \text{ nm}}$ and $N_{3-10 \text{ nm}}$, (b) surface area and $N_{>100 \text{ nm}}$, (c) CH_4 and CO , and (d) RH and UV irradiance from a descending flight leg during RF8 (13 September 2019).

5 Summary

515 In this study, we examine NPF events in the tropical FT in the altitude range of 3–8.5 km using airborne measurements collected during CAMP²Ex campaign. NPF events were classified based on air mass types, including background, biomass burning influenced, and urban influenced. The features of key variables, including RH, surface area, UV irradiance as well as concentrations of trace gases are presented for different NPF types and over different altitude ranges. The impact of air mass types on the NPF is investigated. We summarize key conclusions as follows:

- 520
- 1) Most of the NPF events were observed above 6 km in air that was processed by convective clouds and with low existing aerosol surface area. No newly formed particles were observed below 3 km, possibly due to high temperature and high condensation sink. Below 6 km, NPF was rare and mostly observed in urban



- 525 influenced air, likely due to abundant precursors emitted from urban areas. Above 6 km, NPF frequency increases with altitude, reaching about 49% at 8 km, and NPF frequency in background air was usually higher than in urban influenced air masses. There is a drastic decrease in NPF frequency from the southwest monsoon to the monsoon transition, coinciding with a statistical decrease in RH and increase in surface area in the FT. The decrease of NPF frequency during the monsoon transition phase is attributed to the decrease of convective activity and thus less efficient removal of existing aerosol particles.
- 530 2) NPF in background air was observed under two different types of conditions. One type was observed around noon time in the vicinity of clouds, with high RH (above 70%), reduced surface area, and strong UV irradiance. The second type was observed in the early morning with some of lowest surface area observed during CAMP²Ex. The very low surface area is attributed to a combination of wet-scavenging and less convection (i.e., reduced vertical transport of aerosol particles from near surface to the FT) over night. NPF in the morning is likely made possible by the much lower surface area (i.e., condensation sink for the nucleating species), despite the lower UV irradiance and calculated actinic flux compared to noon time
- 535 periods at the same altitudes.
- 540 3) The impact from biomass burning and urban emissions on NPF is investigated. During CAMP²Ex, the impact of urban emission on NPF shows a clear altitude dependence. Between 5.5 and 7 km, urban influenced and biomass burning influenced NPF were observed with reduced surface area and enhanced UV irradiance near clouds. The elevated concentrations of precursors from either urban emission or biomass burning enhances the formation of nucleating species and NPF. Urban-influenced NPF was usually observed close to the land where the influence of fresh urban emissions is expected.
- 545 4) Above 7 km, urban influenced NPF was observed when the background humid air was lifted by convective clouds and mixed into the aged urban plume. The reactive precursors in the aged urban plume were mostly consumed during the long-range transport from East Asia, while existing particle surface area remained relatively high due to longer aerosol lifetime in the FT. As a result, the aged urban plume tends to inhibit NPF instead of promoting it as is the case with air masses influenced by fresh urban emissions at lower altitudes.
- 550 5) A small number of urban-influenced NPF events were observed with high existing aerosol surface area. The vertical profile of particle number concentrations indicates that the small particles were formed in the detrainment layers instead of originating from the primary emissions near the surface. High concentrations of precursors from urban emissions likely made NPF possible despite relatively high existing surface area.

555 The results from this study highlight the role of convective clouds that efficiently scavenge existing aerosol particles, inject reactive precursors into the FT, and enhance UV irradiance, all of which facilitate nucleation and particle formation. The results also show competing influences of different variables and complex interactions between anthropogenic emissions, transport, convective clouds, and meteorology, which lead to NPF under a variety of conditions and altitudes. Due to the lack of measurements of precursors, the nucleation pathways of NPF in different air mass types are not well understood and should be examined in future studies. The impact of urban and



560 biomass burning emissions on NPF, and subsequent formation of cloud condensation nuclei will also need to be examined in the future by combining field observations and model simulations.

Data Availability. CAMP²Ex observational datasets are available at <https://asdc.larc.nasa.gov/project/CAMP2Ex>. HYSPLIT data are accessible through the NOAA READY website (<http://www.ready.noaa.gov>).

565 *Author Contributions.* JW and QX designed the study. JZ, YW, LZ, EC, EW, CR, JD, GD, KS, SW, SS, and PL carried out the measurements and data reduction. QX and JW led the data analysis and the preparation of manuscript, with contributions from all authors. We thank Michael Jones and Adam Bell for their comments on the manuscript.

Competing interests. One of the co-authors is a member of the editorial board of *Atmospheric Chemistry and Physics*. The peer-review process was guided by an independent editor, and the authors have also no other competing interests to declare.

570 *Acknowledgement.* We acknowledge the funding support from National Aeronautics and Space Administration (grant no. 80NSSC19K0618).



References

- Ahern, A. T., Robinson, E. S., Tkacik, D. S., Saleh, R., Hatch, L. E., Barsanti, K. C., Stockwell, C. E., Yokelson, R. J., Presto, A. A., Robinson, A. L., Sullivan, R. C., and Donahue, N. M.: Production of Secondary Organic Aerosol During Aging of Biomass Burning Smoke From Fresh Fuels and Its Relationship to VOC Precursors, *Journal of Geophysical Research: Atmospheres*, 124, 3583-3606, <https://doi.org/10.1029/2018JD029068>, 2019.
- 575
- Akherati, A., He, Y., Coggon, M. M., Koss, A. R., Hodshire, A. L., Sekimoto, K., Warneke, C., de Gouw, J., Yee, L., Seinfeld, J. H., Onasch, T. B., Herndon, S. C., Knighton, W. B., Cappa, C. D., Kleeman, M. J., Lim, C. Y., Kroll, J. H., Pierce, J. R., and Jathar, S. H.: Oxygenated Aromatic Compounds are Important Precursors of Secondary Organic Aerosol in Biomass-Burning Emissions, *Environmental Science & Technology*, 54, 8568-8579, [10.1021/acs.est.0c01345](https://doi.org/10.1021/acs.est.0c01345), 2020.
- 580
- Alam, A., Shi, J. P., and Harrison, R. M.: Observations of new particle formation in urban air, *Journal of Geophysical Research: Atmospheres*, 108, <https://doi.org/10.1029/2001JD001417>, 2003.
- Andreae, M. O., Afchine, A., Albrecht, R., Holanda, B. A., Artaxo, P., Barbosa, H. M. J., Borrmann, S., Cecchini, M. A., Costa, A., Dollner, M., Fütterer, D., Järvinen, E., Jurkat, T., Klimach, T., Konemann, T., Knote, C., Krämer, M., Krisna, T., Machado, L. A. T., Mertes, S., Minikin, A., Pöhlker, C., Pöhlker, M. L., Pöschl, U., Rosenfeld, D., Sauer, D., Schlager, H., Schnaiter, M., Schneider, J., Schulz, C., Spanu, A., Sperling, V. B., Voigt, C., Walser, A., Wang, J., Weinzierl, B., Wendisch, M., and Ziereis, H.: Aerosol characteristics and particle production in the upper troposphere over the Amazon Basin, *Atmos. Chem. Phys.*, 18, 921-961, [10.5194/acp-18-921-2018](https://doi.org/10.5194/acp-18-921-2018), 2018.
- 585
- Arthur, D. and Vassilvitskii, S.: k-means++: the advantages of careful seeding, *Proceedings of the eighteenth annual ACM-SIAM symposium on Discrete algorithms*, New Orleans, Louisiana 2007.
- 590
- Baier, B. C., Sweeney, C., Choi, Y., Davis, K. J., DiGangi, J. P., Feng, S., Fried, A., Halliday, H., Higgs, J., and Lauvaux, T.: Multispecies assessment of factors influencing regional CO₂ and CH₄ enhancements during the winter 2017 ACT-America campaign, *Journal of Geophysical Research: Atmospheres*, 125, e2019JD031339, 2020.
- 595
- Chae, J. H., Wu, D. L., Read, W. G., and Sherwood, S. C.: The role of tropical deep convective clouds on temperature, water vapor, and dehydration in the tropical tropopause layer (TTL), *Atmos. Chem. Phys.*, 11, 3811-3821, [10.5194/acp-11-3811-2011](https://doi.org/10.5194/acp-11-3811-2011), 2011.
- Chen, H., Schmidt, S., King, M. D., Wind, G., Bucholtz, A., Reid, E. A., Segal-Rozenhaimer, M., Smith, W. L., Taylor, P. C., Kato, S., and Pilewskie, P.: The effect of low-level thin arctic clouds on shortwave irradiance: evaluation of estimates from spaceborne passive imagery with aircraft observations, *Atmos. Meas. Tech.*, 14, 2673-2697, [10.5194/amt-14-2673-2021](https://doi.org/10.5194/amt-14-2673-2021), 2021.
- 600
- Clarke, A. D., Vamer, J. L., Eisele, F., Mauldin, R. L., Tanner, D., and Litchy, M.: Particle production in the remote marine atmosphere: Cloud outflow and subsidence during ACE 1, *Journal of Geophysical Research: Atmospheres*, 103, 16397-16409, <https://doi.org/10.1029/97JD02987>, 1998.



- 605 Clarke, A. D., Eisele, F., Kapustin, V., Moore, K., Tanner, D., Mauldin, R., Litchy, M., Lienert, B., Carroll, M. A., and Albercook, G.: Nucleation in the equatorial free troposphere: Favorable environments during PEM-Tropics, *Journal of Geophysical Research*, 104, 5735-5744, 10.1029/98JD02303, 1999.
- Corral, A. F., Choi, Y., Crosbie, E., Dadashazar, H., DiGangi, J. P., Diskin, G. S., Fenn, M., Harper, D. B., Kirschler, S., Liu, H., Moore, R. H., Nowak, J. B., Scarino, A. J., Seaman, S., Shingler, T., Shook, M. A., Thornhill,
- 610 K. L., Voigt, C., Zhang, B., Ziemba, L. D., and Sorooshian, A.: Cold Air Outbreaks Promote New Particle Formation Off the U.S. East Coast, *Geophysical Research Letters*, 49, e2021GL096073, <https://doi.org/10.1029/2021GL096073>, 2022.
- Crutzen, P. J. and Andreae, M. O.: Biomass Burning in the Tropics: Impact on Atmospheric Chemistry and Biogeochemical Cycles, *Science*, 250, 1669-1678, doi:10.1126/science.250.4988.1669, 1990.
- 615 Dada, L., Paasonen, P., Nieminen, T., Buenrostro Mazon, S., Kontkanen, J., Peräkylä, O., Lehtipalo, K., Hussein, T., Petäjä, T., Kerminen, V. M., Bäck, J., and Kulmala, M.: Long-term analysis of clear-sky new particle formation events and nonevents in Hyytiälä, *Atmos. Chem. Phys.*, 17, 6227-6241, 10.5194/acp-17-6227-2017, 2017.
- Dadashazar, H., Braun, R. A., Crosbie, E., Chuang, P. Y., Woods, R. K., Jonsson, H. H., and Sorooshian, A.: Aerosol characteristics in the entrainment interface layer in relation to the marine boundary layer and free
- 620 troposphere, *Atmos. Chem. Phys.*, 18, 1495-1506, 10.5194/acp-18-1495-2018, 2018.
- DiGangi, J. P., Choi, Y., Nowak, J. B., Halliday, H. S., Diskin, G. S., Feng, S., Barkley, Z. R., Lauvaux, T., Pal, S., Davis, K. J., Baier, B. C., and Sweeney, C.: Seasonal Variability in Local Carbon Dioxide Biomass Burning Sources Over Central and Eastern US Using Airborne In Situ Enhancement Ratios, *Journal of Geophysical Research: Atmospheres*, 126, e2020JD034525, <https://doi.org/10.1029/2020JD034525>, 2021.
- 625 Diskin, G., Podolske, J., Sachse, G., and Slate, T.: Open-path airborne tunable diode laser hygrometer, *International Symposium on Optical Science and Technology*, SPIE2002.
- Dunne, E. M., Gordon, H., Kürten, A., Almeida, J., Duplissy, J., Williamson, C., Ortega, I. K., Pringle, K. J., Adamov, A., Baltensperger, U., Barmet, P., Benduhn, F., Bianchi, F., Breitenlechner, M., Clarke, A., Curtius, J., Dommen, J., Donahue, N. M., Ehrhart, S., Flagan, R. C., Franchin, A., Guida, R., Hakala, J., Hansel, A., Heinritzi,
- 630 M., Jokinen, T., Kangasluoma, J., Kirkby, J., Kulmala, M., Kupc, A., Lawler, M. J., Lehtipalo, K., Makhmutov, V., Mann, G., Mathot, S., Merikanto, J., Miettinen, P., Nenes, A., Onnela, A., Rap, A., Reddington, C. L. S., Riccobono, F., Richards, N. A. D., Rissanen, M. P., Rondo, L., Sarnela, N., Schobesberger, S., Sengupta, K., Simon, M., Sipilä, M., Smith, J. N., Stozkhov, Y., Tomé, A., Tröstl, J., Wagner, P. E., Wimmer, D., Winkler, P. M., Worsnop, D. R., and Carslaw, K. S.: Global atmospheric particle formation from CERN CLOUD measurements, *Science*, 354, 1119-
- 635 1124, doi:10.1126/science.aaf2649, 2016.
- Fiedler, V., Arnold, F., Ludmann, S., Minikin, A., Hamburger, T., Pirjola, L., Dörnbrack, A., and Schlager, H.: African biomass burning plumes over the Atlantic: aircraft based measurements and implications for



- H₂SO₄ and HNO₃ mediated smoke particle activation, *Atmos. Chem. Phys.*, 11, 3211-3225, 10.5194/acp-11-3211-2011, 2011.
- 640 Gilman, J. B., Lerner, B. M., Kuster, W. C., Goldan, P. D., Warneke, C., Veres, P. R., Roberts, J. M., de Gouw, J. A., Burling, I. R., and Yokelson, R. J.: Biomass burning emissions and potential air quality impacts of volatile organic compounds and other trace gases from fuels common in the US, *Atmos. Chem. Phys.*, 15, 13915-13938, 10.5194/acp-15-13915-2015, 2015.
- Gordon, H., Kirkby, J., Baltensperger, U., Bianchi, F., Breitenlechner, M., Curtius, J., Dias, A., Dommen, J.,
645 Donahue, N. M., Dunne, E. M., Duplissy, J., Ehrhart, S., Flagan, R. C., Frege, C., Fuchs, C., Hansel, A., Hoyle, C. R., Kulmala, M., Kürten, A., Lehtipalo, K., Makhmutov, V., Molteni, U., Rissanen, M. P., Stozkhov, Y., Tröstl, J., Tsagkogeorgas, G., Wagner, R., Williamson, C., Wimmer, D., Winkler, P. M., Yan, C., and Carslaw, K. S.: Causes and importance of new particle formation in the present-day and preindustrial atmospheres, *Journal of Geophysical Research: Atmospheres*, 122, 8739-8760, <https://doi.org/10.1002/2017JD026844>, 2017.
- 650 Hamed, A., Korhonen, H., Sihto, S.-L., Joutsensaari, J., Järvinen, H., Petäjä, T., Arnold, F., Nieminen, T., Kulmala, M., Smith, J. N., Lehtinen, K. E. J., and Laaksonen, A.: The role of relative humidity in continental new particle formation, *Journal of Geophysical Research: Atmospheres*, 116, <https://doi.org/10.1029/2010JD014186>, 2011.
- Hegg, D. A., Radke, L. F., Hobbs, P. V., and Riggan, P. J.: Ammonia emissions from biomass burning, *Geophysical Research Letters*, 15, 335-337, <https://doi.org/10.1029/GL015i004p00335>, 1988.
- 655 Helfter, C., Tremper, A. H., Halios, C. H., Kotthaus, S., Björkegren, A., Grimmond, C. S. B., Barlow, J. F., and Nemitz, E.: Spatial and temporal variability of urban fluxes of methane, carbon monoxide and carbon dioxide above London, UK, *Atmos. Chem. Phys.*, 16, 10543-10557, 10.5194/acp-16-10543-2016, 2016.
- Hennigan, C. J., Westervelt, D. M., Riipinen, I., Engelhart, G. J., Lee, T., Collett Jr., J. L., Pandis, S. N., Adams, P. J., and Robinson, A. L.: New particle formation and growth in biomass burning plumes: An important source of
660 cloud condensation nuclei, *Geophysical Research Letters*, 39, <https://doi.org/10.1029/2012GL050930>, 2012.
- Hermann, M., Wehner, B., Bischof, O., Han, H. S., Krinke, T., Liu, W., Zerrath, A., and Wiedensohler, A.: Particle counting efficiencies of new TSI condensation particle counters, *Journal of Aerosol Science*, 38, 674-682, <https://doi.org/10.1016/j.jaerosci.2007.05.001>, 2007.
- Hilario, M. R. A., Cruz, M. T., Cambaliza, M. O. L., Reid, J. S., Xian, P., Simpas, J. B., Lagrosas, N. D., Uy, S. N.
665 Y., Cliff, S., and Zhao, Y.: Investigating size-segregated sources of elemental composition of particulate matter in the South China Sea during the 2011 Vasco cruise, *Atmos. Chem. Phys.*, 20, 1255-1276, 10.5194/acp-20-1255-2020, 2020.
- Hilario, M. R. A., Crosbie, E., Shook, M., Reid, J. S., Cambaliza, M. O. L., Simpas, J. B. B., Ziemba, L., DiGangi, J. P., Diskin, G. S., Nguyen, P., Turk, F. J., Winstead, E., Robinson, C. E., Wang, J., Zhang, J., Wang, Y., Yoon, S.,
670 Flynn, J., Alvarez, S. L., Behrangi, A., and Sorooshian, A.: Measurement report: Long-range transport patterns into



- the tropical northwest Pacific during the CAMP2Ex aircraft campaign: chemical composition, size distributions, and the impact of convection, *Atmos. Chem. Phys.*, 21, 3777-3802, 10.5194/acp-21-3777-2021, 2021.
- Hodshire, A. L., Ramnarine, E., Akherati, A., Alvarado, M. L., Farmer, D. K., Jathar, S. H., Kreidenweis, S. M., Lonsdale, C. R., Onasch, T. B., Springston, S. R., Wang, J., Wang, Y., Kleinman, L. I., Sedlacek Iii, A. J., and
675 Pierce, J. R.: Dilution impacts on smoke aging: evidence in Biomass Burning Observation Project (BBOP) data, *Atmos. Chem. Phys.*, 21, 6839-6855, 10.5194/acp-21-6839-2021, 2021.
- Kazil, J., Lovejoy, E. R., Barth, M. C., and O'Brien, K.: Aerosol nucleation over oceans and the role of galactic cosmic rays, *Atmos. Chem. Phys.*, 6, 4905-4924, 10.5194/acp-6-4905-2006, 2006.
- Kerminen, V.-M., Chen, X., Vakkari, V., Petäjä, T., Kulmala, M., and Bianchi, F.: Atmospheric new particle
680 formation and growth: review of field observations, *Environmental Research Letters*, 13, 103003, 2018.
- Kuang, C., McMurry, P. H., and McCormick, A. V.: Determination of cloud condensation nuclei production from measured new particle formation events, *Geophysical Research Letters*, 36, <https://doi.org/10.1029/2009GL037584>, 2009.
- Kulmala, M., Petäjä, T., Ehn, M., Thornton, J., Sipilä, M., Worsnop, D. R., and Kerminen, V.-M.: Chemistry of
685 Atmospheric Nucleation: On the Recent Advances on Precursor Characterization and Atmospheric Cluster Composition in Connection with Atmospheric New Particle Formation, *Annual Review of Physical Chemistry*, 65, 21-37, 10.1146/annurev-physchem-040412-110014, 2014.
- Lawson, P., Gurganus, C., Woods, S., and Bruintjes, R.: Aircraft Observations of Cumulus Microphysics Ranging from the Tropics to Midlatitudes: Implications for a "New" Secondary Ice Process, *Journal of the Atmospheric
690 Sciences*, 74, 2899-2920, 10.1175/jas-d-17-0033.1, 2017.
- Lee, S. H., Young, L.-H., Benson, D. R., Suni, T., Kulmala, M., Junninen, H., Campos, T. L., Rogers, D. C., and Jensen, J. B.: Observations of nighttime new particle formation in the troposphere, *Journal of Geophysical Research*, 113, 2008.
- Lloyd, S.: Least squares quantization in PCM, *IEEE Transactions on Information Theory*, 28, 129-137,
695 10.1109/TIT.1982.1056489, 1982.
- Meinardi, S., Simpson, I. J., Blake, N. J., Blake, D. R., and Rowland, F. S.: Dimethyl disulfide (DMDS) and dimethyl sulfide (DMS) emissions from biomass burning in Australia, *Geophysical Research Letters*, 30, <https://doi.org/10.1029/2003GL016967>, 2003.
- Nara, H., Tanimoto, H., Tohjima, Y., Mukai, H., Nojiri, Y., and Machida, T.: Emission factors of CO₂, CO and CH₄
700 from Sumatran peatland fires in 2013 based on shipboard measurements, *Tellus B Chem Phys Meteorol*, 69, 10.1080/16000889.2017.1399047, 2017.



- Norgren, M. S., Wood, J., Schmidt, K. S., van Dierenhoven, B., Stamnes, S. A., Ziemba, L. D., Crosbie, E. C., Shook, M. A., Kittelman, A. S., LeBlanc, S. E., Broccardo, S., Freitag, S., and Reid, J. S.: Above-aircraft cirrus cloud and aerosol optical depth from hyperspectral irradiances measured by a total-diffuse radiometer, *Atmos. Meas. Tech.*, 15, 1373-1394, 10.5194/amt-15-1373-2022, 2022.
- 705
- Perry, K. D. and Hobbs, P. V.: Further evidence for particle nucleation in clear air adjacent to marine cumulus clouds, *Journal of Geophysical Research: Atmospheres*, 99, 22803-22818, <https://doi.org/10.1029/94JD01926>, 1994.
- Pirjola, L., O'Dowd, C. D., Brooks, I. M., and Kulmala, M.: Can new particle formation occur in the clean marine boundary layer?, *Journal of Geophysical Research: Atmospheres*, 105, 26531-26546, <https://doi.org/10.1029/2000JD900310>, 2000.
- 710
- Podolske, J. R., Sachse, G. W., and Diskin, G. S.: Calibration and data retrieval algorithms for the NASA Langley/Ames Diode Laser Hygrometer for the NASA transport and chemical evolution over the pacific (TRACE-P) mission, *Journal of Geophysical Research: Atmospheres*, 108, 2003.
- Reid, J. S., Posselt, D. J., Kaku, K., Holz, R. A., Chen, G., Eloranta, E. W., Kuehn, R. E., Woods, S., Zhang, J., Anderson, B., Bui, T. P., Diskin, G. S., Minnis, P., Newchurch, M. J., Tanelli, S., Trepte, C. R., Thornhill, K. L., and Ziemba, L. D.: Observations and hypotheses related to low to middle free tropospheric aerosol, water vapor and altocumulus cloud layers within convective weather regimes: a SEAC4RS case study, *Atmos. Chem. Phys.*, 19, 11413-11442, 10.5194/acp-19-11413-2019, 2019.
- 715
- Reid, J. S., Lagrosas, N. D., Jonsson, H. H., Reid, E. A., Atwood, S. A., Boyd, T. J., Ghate, V. P., Xian, P., Posselt, D. J., Simpas, J. B., Uy, S. N., Zaiger, K., Blake, D. R., Bucholtz, A., Campbell, J. R., Chew, B. N., Cliff, S. S., Holben, B. N., Holz, R. E., Hyer, E. J., Kreidenweis, S. M., Kuciauskas, A. P., Lolli, S., Oo, M., Perry, K. D., Salinas, S. V., Sessions, W. R., Smirnov, A., Walker, A. L., Wang, Q., Yu, L., Zhang, J., and Zhao, Y.: Aerosol meteorology of Maritime Continent for the 2012 7SEAS southwest monsoon intensive study – Part 2: Philippine receptor observations of fine-scale aerosol behavior, *Atmos. Chem. Phys.*, 16, 14057-14078, 10.5194/acp-16-14057-2016, 2016.
- 720
- Rousseuw, P. J.: Silhouettes: A graphical aid to the interpretation and validation of cluster analysis, *Journal of Computational and Applied Mathematics*, 20, 53-65, [https://doi.org/10.1016/0377-0427\(87\)90125-7](https://doi.org/10.1016/0377-0427(87)90125-7), 1987.
- Schmidt, K. S., Wendisch, M., and Kindel, B.: Airborne Solar Radiation Sensors, in: *Springer Handbook of Atmospheric Measurements*, edited by: Foken, T., Springer International Publishing, Cham, 1131-1150, 10.1007/978-3-030-52171-4_40, 2021.
- 730
- Shang, D., Hu, M., Zheng, J., Qin, Y., Du, Z., Li, M., Fang, J., Peng, J., Wu, Y., Lu, S., and Guo, S.: Particle number size distribution and new particle formation under the influence of biomass burning at a high altitude background site at Mt. Yulong (3410&thinspm), China, *Atmos. Chem. Phys.*, 18, 15687-15703, 10.5194/acp-18-15687-2018, 2018.



- 735 Spracklen, D. V., Carslaw, K. S., Pöschl, U., Rap, A., and Forster, P. M.: Global cloud condensation nuclei influenced by carbonaceous combustion aerosol, *Atmos. Chem. Phys.*, 11, 9067-9087, 10.5194/acp-11-9067-2011, 2011.
- Syakur, M. A., Khotimah, B. K., Rochman, E. M. S., and Satoto, B. D.: Integration K-Means Clustering Method and Elbow Method For Identification of The Best Customer Profile Cluster, *IOP Conference Series: Materials Science and Engineering*, 336, 012017, 10.1088/1757-899x/336/1/012017, 2018.
- 740 Twohy, C. H., Clement, C. F., Gandrud, B. W., Weinheimer, A. J., Campos, T. L., Baumgardner, D., Brune, W. H., Faloon, I., Sachse, G. W., Vay, S. A., and Tan, D.: Deep convection as a source of new particles in the midlatitude upper troposphere, *Journal of Geophysical Research: Atmospheres*, 107, AAC 6-1-AAC 6-10, <https://doi.org/10.1029/2001JD000323>, 2002.
- 745 Uhrner, U., Zallinger, M., von Löwis, S., Vehkamäki, H., Wehner, B., Stratmann, F., and Wiedensohler, A.: Volatile Nanoparticle Formation and Growth within a Diluting Diesel Car Exhaust, *Journal of the Air & Waste Management Association*, 61, 399-408, 10.3155/1047-3289.61.4.399, 2011.
- Vakkari, V., Beukes, J. P., Dal Maso, M., Aurela, M., Josipovic, M., and van Zyl, P. G.: Major secondary aerosol formation in southern African open biomass burning plumes, *Nature Geoscience*, 11, 580-583, 10.1038/s41561-018-0170-0, 2018.
- 750 Vehkamäki, H., Kulmala, M., Napari, I., Lehtinen, K. E. J., Timmreck, C., Noppel, M., and Laaksonen, A.: An improved parameterization for sulfuric acid–water nucleation rates for tropospheric and stratospheric conditions, *Journal of Geophysical Research: Atmospheres*, 107, AAC 3-1-AAC 3-10, <https://doi.org/10.1029/2002JD002184>, 2002.
- 755 Wang, J., Pikridas, M., Spielman, S. R., and Pinterich, T.: A fast integrated mobility spectrometer for rapid measurement of sub-micrometer aerosol size distribution, Part I: Design and model evaluation, *Journal of Aerosol Science*, 108, 44-55, 2017a.
- Wang, J., Pikridas, M., Pinterich, T., Spielman, S. R., Tsang, T., McMahon, A., and Smith, S.: A Fast Integrated Mobility Spectrometer for rapid measurement of sub-micrometer aerosol size distribution, Part II: Experimental characterization, *Journal of Aerosol Science*, 113, 119-129, <https://doi.org/10.1016/j.jaerosci.2017.05.001>, 2017b.
- 760 Wang, Y., Pinterich, T., and Wang, J.: Rapid measurement of sub-micrometer aerosol size distribution using a fast integrated mobility spectrometer, *Journal of Aerosol Science*, 121, 12-20, <https://doi.org/10.1016/j.jaerosci.2018.03.006>, 2018.
- 765 Wehner, B., Uhrner, U., von Löwis, S., Zallinger, M., and Wiedensohler, A.: Aerosol number size distributions within the exhaust plume of a diesel and a gasoline passenger car under on-road conditions and determination of emission factors, *Atmospheric Environment*, 43, 1235-1245, <https://doi.org/10.1016/j.atmosenv.2008.11.023>, 2009.



- Wehner, B., Werner, F., Ditas, F., Shaw, R. A., Kulmala, M., and Siebert, H.: Observations of new particle formation in enhanced UV irradiance zones near cumulus clouds, *Atmos. Chem. Phys.*, 15, 11701-11711, 10.5194/acp-15-11701-2015, 2015.
- 770 Williamson, C. J., Kupe, A., Axisa, D., Bilsback, K. R., Bui, T., Campuzano-Jost, P., Dollner, M., Froyd, K. D., Hodshire, A. L., Jimenez, J. L., Kodros, J. K., Luo, G., Murphy, D. M., Nault, B. A., Ray, E. A., Weinzierl, B., Wilson, J. C., Yu, F., Yu, P., Pierce, J. R., and Brock, C. A.: A large source of cloud condensation nuclei from new particle formation in the tropics, *Nature*, 574, 399-403, 10.1038/s41586-019-1638-9, 2019.
- 775 Worden, J. R., Bloom, A. A., Pandey, S., Jiang, Z., Worden, H. M., Walker, T. W., Houweling, S., and Röckmann, T.: Reduced biomass burning emissions reconcile conflicting estimates of the post-2006 atmospheric methane budget, *Nature Communications*, 8, 2227, 10.1038/s41467-017-02246-0, 2017.
- Xian, P., Reid, J. S., Atwood, S. A., Johnson, R. S., Hyer, E. J., Westphal, D. L., and Sessions, W.: Smoke aerosol transport patterns over the Maritime Continent, *Atmospheric Research*, 122, 469-485, <https://doi.org/10.1016/j.atmosres.2012.05.006>, 2013.
- 780 Yee, L. D., Kautzman, K. E., Loza, C. L., Schilling, K. A., Coggon, M. M., Chhabra, P. S., Chan, M. N., Chan, A. W. H., Hersey, S. P., Crouse, J. D., Wennberg, P. O., Flagan, R. C., and Seinfeld, J. H.: Secondary organic aerosol formation from biomass burning intermediates: phenol and methoxyphenols, *Atmos. Chem. Phys.*, 13, 8019-8043, 10.5194/acp-13-8019-2013, 2013.
- 785 Zhang, R., Khalizov, A., Wang, L., Hu, M., and Xu, W.: Nucleation and Growth of Nanoparticles in the Atmosphere, *Chemical Reviews*, 112, 1957-2011, 10.1021/cr2001756, 2012.
- Zheng, G., Wang, Y., Wood, R., Jensen, M. P., Kuang, C., McCoy, I. L., Matthews, A., Mei, F., Tomlinson, J. M., and Shilling, J. E.: New particle formation in the remote marine boundary layer, *Nature communications*, 12, 1-10, 2021.
- 790 Zhu, Y., Sabaliauskas, K., Liu, X., Meng, H., Gao, H., Jeong, C.-H., Evans, G. J., and Yao, X.: Comparative analysis of new particle formation events in less and severely polluted urban atmosphere, *Atmospheric Environment*, 98, 655-664, <https://doi.org/10.1016/j.atmosenv.2014.09.043>, 2014.